The receptor-like kinase BIR1 inhibits elicitor-induced plasmodesmata callose deposition and PTI gene expression and requires EDS1 and SOBIR1 to cause dose-dependent cell-death in Arabidopsis

Irene Guzmán-Benito[1], Carmen Robinson[1], Chenlei Hua[2], Ana Rocio Sede[3], Laura Elvira-González[3], Isabel Punzón[1], Manfred Heinlein[3], Thorsten Nürnberger[2], César Llave[1]*

[1]Centro de Investigaciones Biológicas Margarita Salas. Consejo Superior de Investigaciones Científicas, Ramiro de Maeztu 9, 28040 Madrid, Spain; [2]Department of Plant Biochemistry, Center of Plant Molecular Biology (ZMBP), University of Tübingen, Tübingen, Germany; [3]Institut de Biologie Moléculaire des Plantes, CNRS, Université de Strasbourg, 67000 Strasbourg, France

Author for correspondence: César Llave

E-mail: cesarllave@cib.csic.es

Phone: +34-91-8373112

WORD COUNT:
Summary: 184
Introduction: 1,061
Materials and methods: 1,347
Results: 3,930
Discussion: 1,484
Acknowledgments: 73

Number of figures: 7
Number of figures in color: 7

Supporting information

Number of supporting figures: 7

Number of supporting tables: 7

Summary

- The receptor-like kinase BIR1 functions as a negative regulator of cell death and defense in Arabidopsis. Previous studies showed that BIR1 expression is up-regulated during infections with microbes and viruses. However, the biological consequences of BIR1 induction remain unknown.
- Here, we use a DEX-inducible expression system in Arabidopsis to investigate the outputs associated with physiological and non-physiological levels of BIR1 expression.
- We show that BIR1 induction at physiological levels significantly interferes with gene expression and plasmodesmata callose deposition triggered by canonical PTI elicitors. We found that plants that accumulated non-physiological doses of BIR1 displayed morphological defects that concur with transcriptomic changes in multiple plant defense genes. We provide experimental evidence that EDS1 and SOBIR1 are required for the ETI-type cell death phenotypes associated to non-physiological levels of BIR1
- Here we propose that BIR1 induction may represent a pathogen-triggered mechanism to modulate plant defenses during infection. Our model posits that when BIR1 regulation is lost, BIR1 integrity is sensed by one or several guarding resistance (R) proteins to initiate an ETI-like response, in which SOBIR1 cooperates with EDS1 to transduce signals downstream of R proteins.

Key words

Arabidopsis, immune regulation, immune receptor, cell death, BAK1-INTERACTING RECEPTOR-LIKE KINASE 1 (BIR1), SUPPRESSOR OF BIR1 (SOBIR1), ENHANCED DISEASE SUSCEPTIBILITY 1 (EDS1)

Introduction

Plants use immunity to defend themselves against invaders such as bacteria, fungi, oomycetes, and viruses (Korner *et al.*, 2013; Macho & Lozano-Duran, 2019; Nishad *et al.*, 2020; Ngou *et al.*, 2022). This system involves multiple cell-surface pattern recognition receptors (PRR) that recognize pathogen/microbe/damage-associated molecular patterns (PAMP/MAMP/DAMP), leading to pattern-triggered immunity (PTI), and intracellular receptors that sense pathogen-effector proteins or effector-induced manipulations of host proteins, leading to effector-triggered immunity (ETI) (Li *et al.*, 2020; Zhou & Zhang, 2020; Lee *et al.*, 2021; Yu *et al.*, 2021). PRRs are single-transmembrane receptor-like kinases (RLK) or receptor-like proteins (RLP), which form active receptor complexes in a ligand-dependent manner with members of the somatic embryogenesis co-receptor kinases (SERKs), including BRASSINOSTEROID INSENSITIVE1-ASSOCIATED RECEPTOR KINASE 1 (BAK1/SERK3) (Boutrot & Zipfel, 2017; Hohmann *et al.*, 2017; Tang *et al.*, 2017; Smakowska-Luzan *et al.*, 2018; Lee *et al.*, 2021). BAK1 functions as a positive regulator of PTI (Liebrand *et al.*, 2014; Wu *et al.*, 2020), and has a dual role as positive and negative regulator of cell death during ETI (Belkhadir *et al.*, 2012; Dominguez-Ferreras *et al.*, 2015). RLP-type PRRs lack kinase activity and constitutively associate in a ligand-independent manner with the leucine-rich repeat (LRR)-RLK adapter SUPPRESSOR OF BIR1-1 (SOBIR1) (Gust *et al.*, 2017). Once the microbe is sensed, PRR receptor complexes activate, via trans-phosphorylation, receptor-like cytoplasmic kinases (RLCKs) that initiate downstream signaling cascades (Tang *et al.*, 2017; Liang & Zhou, 2018; Rao *et al.*, 2018). Among them, BOTRYTIS INDUCED KINASE1 (BIK1) functions either as a positive regulator of immunity triggered by LRR-RLKs such as those induced by the flg22 peptide derived from bacterial flagellin (FLAGELLIN SENSING 2, FLS2), or as a negative regulator of immunity triggered by LRR-RLPs such as those induced by the nlp20 fragment of NECROSIS AND ETHYLENE-INDUCING PEPTIDE 1 (NEP1)-LIKE proteins (NLP, RLP23) (Bi *et al.*, 2018; Wan *et al.*, 2019).

ETI relies on nucleotide-binding domain LRR intracellular immune receptors (NLRs) encoded by polymorphic disease resistance genes (R). NLRs comprise either proteins with an N-terminal domain similar to the TOLL/INTERLEUKIN RECEPTOR 1 (TIR1) (TIR-NB-LRR, TNL), proteins with a coiled-coil (CC) domain at the N terminus (CC-NB-LRR, CNL) or proteins with a RESISTANCE TO POWDERY MILDEW 8-LIKE DOMAIN (RPW8)-type domain (RNLs) (McHale *et al.*, 2006; van Wersch *et al.*, 2020; Wang & Chai, 2020). NLRs function as "sensors" that recognize effectors, or as "helpers" that act downstream of sensor NLRs in ETI

91 signaling (Jubic *et al.*, 2019). Recent studies demonstrated that PTI and ETI work together to
92 mutually potentiate the immune response (Yuan *et al.*, 2021b; Yuan *et al.*, 2023). For instance,
93 NLR-mediated signaling is dependent on multiple PTI-associated components such as BAK1,
94 SOBIR1, or BIK1 in a PTI-independent manner, while TNL genes that are up-regulated during
95 early PTI boost immune responses (Ngou *et al.*, 2021; Tian *et al.*, 2021; Yuan *et al.*, 2021a).
96 ENHANCED DISEASE SUSCEPTIBILITY (EDS1), which is essential in TNL-mediated
97 immunity, also plays a key role in PTI signaling in response to different microbial elicitors
98 (Pruitt *et al.*, 2021b; Tian *et al.*, 2021). Furthermore, PTI and ETI outputs usually converge,
99 albeit with different amplitude and duration (Yuan *et al.*, 2021b). Early responses include
100 apoplastic reactive oxygen species (ROS) burst, cytosolic calcium (Ca^{+2}) influx and activation
101 of Ca^{+2}-dependent protein kinases (CPK), and activation of mitogen-activated protein kinases
102 (MAPK). This response is followed by the transcriptional activation of defense processes that
103 include accumulation of defense phytohormones, regulation of cell wall and secretome
104 composition, and cellular motion (Li *et al.*, 2020).

105 Plants deploy a variety of mechanisms to protect themselves from the detrimental effects of
106 hyperactivated defenses (Couto & Zipfel, 2016; Withers & Dong, 2017; Mithoe & Menke,
107 2018). BAK1-INTERACTING RECEPTOR-LIKE KINASE (BIR) proteins play a key role in
108 defense attenuation. The current model postulates that, in the absence of microbes, BIR proteins
109 constitutively associate with BAK1, thus maintaining the PRRs in a resting state. During ligand
110 perception, BAK1 dissociates from BIR and becomes accessible to complex with PRR
111 receptors (Gao *et al.*, 2009; Halter *et al.*, 2014; Imkampe *et al.*, 2017). The Arabidopsis genome
112 has four BIR homologs (Halter *et al.*, 2014). BIR1 exerts a tight control of BAK1- and SOBIR1-
113 mediated cell death signaling, presumably related to PRR-RLP-ligand perception (Albert *et al.*,
114 2015; Liu *et al.*, 2016). BIR2 and BIR3 have critical roles in the negative regulation of PRR-
115 mediated PTI (Halter *et al.*, 2014; Imkampe *et al.*, 2017). Unlike BIR2 and BIR3, BIR1
116 possesses phosphorylation activities (Gao *et al.*, 2009). Interestingly, knocking-out BIR1
117 triggers resistance pathways that implicate components of TNL-mediated ETI response,
118 suggesting that loss of BIR1 activates one or several unknown TNL proteins (Gao *et al.*, 2009;
119 Liu *et al.*, 2016; Schulze *et al.*, 2022).

120 BIR1 expression is transcriptionally activated in response to multiple microbial and viral
121 pathogens in a salicylic acid (SA)-dependent manner (Guzman-Benito *et al.*, 2019). To date,
122 the effects of BIR1 induction on the outcome of plant defenses remain largely unknown.
123 However, previous work showed that transgenic overexpression of BIR1 triggers

124 developmental defects and cell death similar to the autoimmune phenotypes observed in *bir1-*
125 *1* mutants (Gao *et al.*, 2009; Guzman-Benito *et al.*, 2019). Although the consequences of BIR1
126 overexpression have not been fully characterized yet, this finding seems to indicate that
127 perturbations in BIR1 homeostasis have severe growth-defense penalties. Clearly, effective
128 strategies for BIR1 regulation are needed to prevent unbearably high levels of BIR1 expression.
129 In this regard, RNA-directed DNA methylation and post-transcriptional RNA silencing regulate
130 levels of BIR1 transcripts when BIR1 is actively transcribed (Guzman-Benito *et al.*, 2019).

131 In this work, we conducted a time-course analysis to investigate the phenotypical outputs
132 associated with physiological and non-physiological levels of BIR1 expression in Arabidopsis
133 plants. We show that physiological induction of BIR1 interferes with the expression of PTI
134 marker genes and plasmodesmata (PD)-associated callose deposition in response to several PTI
135 elicitors, but not with ethylene accumulation or ROS production. Whereas physiological
136 induction of BIR1 has a subtle impact on the plant transcriptome, the morphological and growth
137 defects caused by the sustained expression of BIR1 are concomitant with the transcriptional
138 reprogramming of multiple genes encoding components of PTI and ETI signaling pathways.
139 We found that the cell death phenotypes associated with prolonged BIR1 overexpression
140 require the TNL-associated EDS1 and/or the RLP-co-receptor SOBIR1, but the underlying
141 mechanism is unknown. Finally, our work demonstrates that a well-balanced expression of
142 BIR1 avoids interference with cellular processes of growth and development, and is critical for
143 plant fitness.

144

145 **Material and methods**

146 **Plant material and growth condition**

147 *Arabidopsis thaliana* plants were grown in controlled environmental chambers under long-day
148 conditions (16h day/8h night) at 22°C. Arabidopsis lines used in this study were derived from
149 the Columbia-0 (Col-0) ecotype. Seeds were surface-sterilized and sown on plates containing
150 ½ Murashige and Skoog (MS) medium supplemented with MES (0,5g/L), 1% sucrose and 0,9%
151 Plant agar (Duchefa Biochemie). Seedlings were transferred to soil seven to ten days after
152 germination.

153 Mutants for *bir1-1* and *sobir1-12* were donated by Yuelin Zhang (University of British
154 Columbia, Canada). The Arabidopsis *eds1-2*, *pad4-1* and *eds5-3* alleles were supplied by Jane
155 E. Parker (Max Planck Institute for Plant Breeding Research, Germany). Arabidopsis mutant

156 *bak1-5* was donated by Birgit Kemmerling (Center of Plant Molecular Biology, University of
157 Tübingen, Germany). The *sid2-2* mutant was a gift from Francisco Tenllado (Centro de
158 Investigaciones Biológicas Margarita Salas, CSIC, Spain).

159 Arabidopsis Col-0 transgenic plants expressing a BIR1-mCherry fusion under a dexamethasone
160 (DEX)-inducible gene expression system (BIR1 L6 and BIR1 L9) have already been described
161 (Guzman-Benito *et al.*, 2019). In this study, the same DEX-inducible expression system
162 containing a mCherry-tagged BIR1 (herein BIR1) protein-coding gene was transformed into
163 Arabidopsis mutant backgrounds according to standard floral dipping (Clough & Bent, 1998).
164 Independent homozygous lines were selected in T3 and used for subsequent experiments.
165 Unless otherwise indicated, morphological phenotypes after DEX treatments were investigated
166 in two independent transgenic lines of each genotype.

167 **RNA analysis**

168 Total RNA was extracted using TRIzol reagent (Invitrogen) and treated with DNase I
169 (Invitrogen) following manufacturer's instructions to eliminate genomic DNA traces. One-step
170 quantitative RT-PCR (RT-qPCR) was carried out using Brilliant III Ultra-Fast SYBR Green
171 QRT-PCR Master Mix (Agilent Technologies) in a Rotor-Gene 6000/Rotor-Gene Q real-time
172 PCR machine (Corbett/Qiagen) (Fernandez-Calvino *et al.*, 2016). Relative gene expression was
173 determined using the Delta-delta cycle threshold method and Rotor-Gene 6000 Series Software
174 (Corbett). Transcript levels of the target genes were normalized to the transcript levels of the
175 housekeeping gene *CBP20* (*At5g44200*) as a reference gene. Primers are listed in Table S1.

176 **Protein analysis**

177 Leaf tissue samples were ground in liquid nitrogen in an Eppendorf tube and homogenized in
178 extraction buffer (65 mM Tris-HCl, pH 8; 3% sodium dodecyl sulfate [SDS]; 1% ß-
179 mercaptoethanol; 10% glycerol). Samples were diluted in Laemmli buffer, incubated for 5 min
180 at 95°C, and loaded onto 10% SDS-PAGE protein gels. After electrophoresis, proteins were
181 blotted onto an ECL nitrocellulose membrane (Amersham-Pharmacia), and detected using
182 commercial horseradish peroxide (HRP)-conjugated secondary antibodies and a
183 chemiluminescent substrate (LiteAblot Plus). Primary and secondary antibodies were diluted
184 according to the manufacturer's recommendations. The RFP-Trap (Chromotek) was used for
185 immunoprecipitation of mCherry-tagged BIR1 protein from Arabidopsis leaves following
186 manufacturer's instruction.

187 **RNA and library preparation for transcriptome sequencing**

188 Total RNA was extracted from each sample using the RNeasy plant mini kit (Qiagen) followed
189 by DNase treatment according to manufacturer's instructions. A total of 24 samples, including
190 three biological replicates per treatment, were collected. Each sample consisted of RNA pooled
191 from six individual plants. RNA degradation and contamination were monitored on 1% agarose
192 gels, and BIR1 transcript accumulation was measured by RT-qPCR. The RNA purity and RNA
193 concentration were checked using a Nanodrop spectrophotometer (ThermoFisher Scientific),
194 while the RNA integrity was measured using the Agilent Bioanalyzer 2100 system (Agilent
195 Technologies). Sequencing libraries were generated at NOVOGENE (HK) COMPANY
196 LIMITED (Wan Chai, Hong Kong) (www.novogene.com) using NEBNext® UltraTM RNA
197 Library Prep Kit for Illumina® (New England Biolabs) following manufacturer's
198 recommendations and index codes were added to attribute sequences to each sample. First-
199 strand cDNA from mRNA was synthesized using random hexamer primer and M-MuLV
200 Reverse Transcriptase (RNase H-). Second-strand cDNA synthesis was subsequently
201 performed using DNA Polymerase I and RNase H. NEBNext Adaptors with hairpin loop
202 structure were ligated. In order to select cDNA fragments of preferentially 150~200 bp in
203 length, the library fragments were purified with the AMPure XP system (Beckman Coulter).
204 PCR was done with Phusion High-Fidelity DNA polymerase, Universal PCR primers and Index
205 (X) Primer. PCR products were purified with the AMPure XP system and library quality was
206 assessed on the Agilent Bioanalyzer 2100 system. Clustering of the index-coded samples was
207 performed on a cBot Cluster Generation System using the TruSeq PE Cluster Kit v3-cBot-HS
208 (Illumina) according to the manufacturer's recommendations. Finally, paired-end reads were
209 generated via an Illumina PE150 Hiseq platform at NOVOGENE (HK) COMPANY LIMITED.

210 **Bioinformatics analysis of RNA-Seq data**

211 Clean reads were obtained by removing adaptor tags and reads containing poly-N and low-
212 quality reads from raw data. Paired-end clean reads were mapped to the Arabidopsis TAIR v10
213 reference genome using HISAT2 software. To quantify the gene expression levels, HTSeq
214 v0.6.1 was used to calculate the number of mapped reads of each gene and then normalize the
215 results to the expected number of Fragments Per Kilobase of transcript sequence per Millions
216 of base-pairs sequenced (FPKM). Differential expression analysis between groups (three
217 biological replicates per condition) was performed using DESeq2 R package (1.18.0). The
218 resulting *p-value*s were adjusted using the Benjamini and Hochberg's approach for controlling
219 the False Discovery Rate (FDR). Genes with an adjusted *p-value* ≤0.05 found by DESeq2 were
220 deemed as differentially expressed (DEG). Functional classification of DEGs including Gene

221 Ontology (GO) and KEGG was performed. GO enrichment analysis of DEGs was implemented
222 by tGOseq R package, in which gene length bias was corrected. KOBAS software was used to
223 test the statistical enrichment of DEGs in the KEGG database GO terms and KEGG pathways
224 with corrected *p-value* ≤0.05 were considered significantly enriched by DEGs. The raw data
225 was deposited in the Gene Expression Omnibus under accession number GSE234036.

226 **Reactive oxygen species (ROS) and ethylene measurement**

227 The detection of ROS and ethylene was performed as described (Albert *et al.*, 2015; Wan *et al.*,
228 2019). Approximately 4-wk-old BIR1 L9 or WT Arabidopsis plants were treated with 30 μM
229 DEX (H_2O was used as control) for 4 days at 24 h intervals and leaves were then cut into pieces
230 and left floating on H_2O overnight before measurement. For ROS assays, leaf pieces were
231 analyzed in a 96-well plate containing 20 μM L-012 (Wako Pure Chemical Industries Ltd) and
232 2 μg ml^{-1} peroxidase. Luminescence was measured both before (background) and over 1 h
233 following flg22 (GenScript Biotech) elicitation or mock treatment using a Mithras LB 940
234 luminometer (Berthold Technologies). For ethylene measurement, leaf pieces were incubated
235 in 20 mM MES buffer, pH 5.6 and the indicated elicitor (GenScript Biotech). Ethylene
236 accumulation was measured by gas chromatographic analysis (GC-14A) of 1 ml of the air
237 drawn from the closed tube with a syringe after the indicated incubation time. At least three
238 replicates were performed for all treatments.

239 **Callose staining**

240 Callose staining was carried out as described (Huang *et al.*, 2022; Huang *et al.*, 2023). Briefly,
241 approximately 4-wk-old BIR1 L9 or WT Arabidopsis plants were sprayed with 30 μM DEX
242 (H_2O was used as control) for 4 days at 24 h intervals and then leaf disks were excised and left
243 floating on H_2O. For callose staining, individual leaf disks were soaked with 0,1% aniline blue
244 solution (in 50 mM potassium phosphate buffer, pH 8.0) containing either 0.5 μg μl^{-1} poly(I:C)
245 (Sigma) or 1 μM flg22 (GenScript Biotech). Leaf disks were further evacuated for 1-2 minutes
246 (< 0.8 pa) in a vacuum desiccator. Aniline blue fluorescence was imaged 30 minutes after
247 poly(I:C)/flg22 or control treatment using a Zeiss LSM 780 confocal laser scanning microscope
248 with ZEN 2.3 software (Carl Zeiss) and using a 405 nm diode laser for excitation and filtering
249 the emission at 475-525 nm. mCherry fluorescence was excited at 561 nm filtering the emission
250 at 560-610 nm. 8-bit images were acquired with a Plant-Apochromat 40x/1.4 Oil DIC M27
251 objective. Callose fluorescence intensity was quantified with ImageJ software
252 (http://rsbweb.nih. gov/ij/) using the plug-in calloseQuant (Huang *et al.*, 2022). Callose spots

253 were measured in 3-4 images taken from each leaf disk. If not otherwise mentioned, three leaf
254 discs per plant from three different plants were evaluated for each genotype or condition.
255 Regions of interest (ROIs) selected by calloseQuant were verified visually before measurement.
256 Individual fluorescence intensities that occurred as outliers from the general distribution of
257 fluorescence intensities (<1%) in the sample were excluded from analysis.

258

259 **Results**

260 **BIR1 induction causes dose-dependent transcriptome reprogramming in Arabidopsis**

261 To understand the downstream biological processes and pathways associated with BIR1
262 induction, we conducted a global transcriptome RNA-Seq assay in Arabidopsis WT and BIR1
263 L9 plants that express a DEX-inducible BIR1-mCherry transgene (Guzman-Benito *et al.*,
264 2019). This system proved to be a valuable tool for studying the phenotypic outcomes caused
265 by different levels of BIR1 expression in the absence of pathogen elicitors or effectors. Three-
266 week-old plants were sprayed with a 30 µM DEX solution at 24 h intervals and rosette leaf
267 samples were harvested for next-generation sequencing. Control plants were mock-treated with
268 H_2O. Three biological replicates were used as representative samples for each condition tested
269 in this study: DEX-treated WT (DeWT_), mock-treated WT (MoWT_), DEX-treated BIR1 L9
270 (DeL9_) and mock-treated BIR1 L9 (MoL9_) plants at 4 or 12 days of treatment as indicated
271 **(Table S2)**. We found that BIR1 was induced at physiological levels in DeL9_ samples after 4
272 days of DEX treatment, and plants displayed WT morphologies **(Fig. 1A)**. In contrast, DeL9_
273 plants accumulated high doses of BIR1 (non-physiological), and exhibited a range of growth
274 defects and premature senescence after long BIR1 induction times (12 days of DEX treatment)
275 **(Fig. 1A)** (Guzman-Benito *et al.*, 2019). Principal component analysis (PCA) was used to sort
276 RNA-seq-based transcriptomic data according to gene expression levels. To discard the
277 potential effects of DEX on gene expression, we first compared DEX-treated WT versus DEX-
278 treated BIR1 L9 plants. PC1 defined a distinct separation in the PCA score plot between WT
279 (DeWT_12) and BIR1 L9 (DeL9_12) samples after 12 days of treatment, indicating that the
280 BIR1 expression level was the main source of variance (36.92%) **(Fig. 1B)**. Samples in the
281 DeL9_4 group, which produced physiological levels of BIR1 after 4 days of treatment,
282 clustered in the proximity of non-transgenic DeWT_4 samples, reflecting their similar
283 expression profiles. PC2 seems to highlight a shift in gene expression between samples due to
284 age or developmental stage (22.07%). When DEX-treated BIR1 L9 plants were compared with

285 mock-treated BIR1 L9 plants, the BIR1 expression level was again the dominant source of
286 variance (36.85%) underlying PC1, whereas time was the basis for PC2 (19.57%) separation in
287 the PCA score plot **(Fig. S1A).**

288 We noticed that normalized BIR1 abundance (FPKM) after 12 days of DEX treatment differed
289 between independent BIR1 L9 replicates (DeL9_12), perhaps due to the differences in DEX
290 sensitivity (**Fig. 1A**). The DeL9_12b sample within the DeL9_12 group was located far from
291 the other DeL9_12 samples in the PCA plot, and positioned near the samples within the
292 DeWT_12 or MoL9_12 clusters **(Figs. 1B, S1A)**. Noticeably, DeL9_12b produced fewer BIR1-
293 derived sequencing reads than the other two samples within the DeL9_12 group **(Fig. 1A)**.
294 Thus, we conclude that BIR1 levels contribute to creating heterogeneous transcriptomes
295 between replicates, although other factors such as the severity of the phenotypes caused by
296 BIR1 overexpression may also yield quantitative differences in their expression profiles.

297 Differentially expressed genes (DEG) from different comparisons are presented in **Table S3**. A
298 dramatic impact on the transcriptome was registered in plants that overexpress BIR1 (12 days
299 of DEX treatment) (adjusted *p*-value ≤ 0.05) **(Figs. S1B, S1C)**. Using stricter statistical
300 thresholds ($|\log_2(\text{Fold-Change})| \geq 1$ and adjusted *p*-value ≤ 0.01), 270 and 2,051 DEGs were
301 detected in BIR1 L9 plants after 4 and 12 days of DEX treatment, respectively, relative to the
302 mock-treated controls (DeL9_ vs MoL9_). Of them, 191 and 1,809 genes were up-regulated
303 and 79 and 242 were down-regulated **(Fig. 1C)** (**Table S4)**. 584 and 4,125 genes were distinctly
304 expressed between BIR1 L9 and WT plants after 4 and 12 days of DEX-treatment (DeL9_ vs
305 DeWT_), respectively, of which 220 and 1,815 genes were up-regulated and 364 and 2,310
306 were down-regulated **(Fig. 1C)** (**Table S4)**. These findings indicate that a massive
307 transcriptional reprogramming occurs when BIR1 is overexpressed in Arabidopsis but not when
308 BIR1 is transcriptionally induced at physiological levels.

309 Gene functional enrichment analysis was used to infer biological functions or pathways
310 significantly associated with DEGs. Gene ontology (GO) analysis showed that genes encoding
311 proteins with oxidoreductase activity, transmembrane transport and other metabolic processes
312 or genes related to lipid or carbohydrate metabolism were particularly overrepresented in our
313 whole set of DEGs, including WT and BIR1 L9 plants, after long DEX treatments **(Figs. 1D,**
314 **S1D, S2D) (Table S5)**. Notably, DEGs with kinase activity were only enriched in BIR1
315 overexpressing L9 plants, relative to mock-treated BIR1 L9 plants **(Figs. 1D, S1D)**. The kinase
316 activity GO term was not enriched in DEX- or mock-treated WT plants at any point tested,
317 excluding a DEX effect **(Fig. S2D)**. The Kyoto Encyclopedia of Genes and Genomes (KEGG)

318 pathway analysis showed the enrichment of genes related to several metabolic processes and
319 biosynthesis of secondary metabolites that were specifically regulated after DEX-treatments
320 **(Fig. S3) (Table S6)**. Conversely, DEGs involved in plant hormone signal transduction were
321 significantly enriched only in BIR1 overexpressing BIR1 L9, but not in mock-treated BIR1 L9
322 plants or WT plants exposed to DEX.

323 As indicated above, the implemented experimental approach further allowed us to study the
324 impact of DEX application. Macroscopically, WT plant treated with DEX for 12 days exhibited
325 identical morphology as the mock-treated controls but produced significantly smaller rosettes
326 due to the effects of DEX treatments **(Fig. S2A)**. Changes in gene expression due to DEX
327 treatments in WT plants are listed in **Table S4 (Fig. S2B)**. PCA analysis revealed that the
328 duration of the DEX treatment was the dominant source of variance underlying PC1 (36.80%)
329 in the PCA score plot **(Fig. S2C)**. GO and KEGG analyses revealed a significant enrichment of
330 terms related to oxidoreductase activities and metabolic processes in response to DEX
331 treatments **(Figs. S2D, S3)**.

332

333 **Effects of BIR1 induction on ROS and ethylene production and PTI gene expression in**
334 **response to bacterial elicitors**

335 We wanted to assess the effects of the physiological induction of BIR1 on early events of the
336 PTI response. BIR1 was induced by treating BIR1 plants with a 30 µM DEX solution 4 times
337 at 24h intervals, whereas control plants were mock-treated with H_2O. The luminol-based assay
338 showed that ROS production triggered by 1 µM flg22 was comparable between WT and BIR1
339 L6 and L9 plants **(Fig. 2A)**. Then, we tested the production of the phytohormone ethylene in
340 response to flg22 and nlp20 at concentrations of 1 µM and 100 nM. As expected, ethylene levels
341 were significantly increased in WT, BIR1 L6 and L9 plants in response to flg22 and, to a greater
342 extent, nlp20 at both concentrations tested. However, the induction of BIR1 in DEX-treated
343 plants had no measurable consequences on ethylene accumulation compared to the mock-
344 treated controls **(Fig. 2B)**. Next, we tested the expression of the canonical PTI marker genes
345 encoding FLG22-INDUCED RECEPTOR-LIKE KINASE 1 (FRK1) and PATHOGENESIS-
346 RELATED 1 (PR1) in BIR1 L6 and L9 transgenic plants upon 1 µM flg22 elicitation. Whereas
347 all these genes were significantly up-regulated in mock-treated controls (DEX-), BIR1
348 induction by DEX in BIR1 L6 an L9 plants notably reduced transcript levels (DEX+).
349 Importantly, PTI genes clearly responded to flg22 in WT plants regardless of DEX, which

350 discards a potential repressive effect of DEX on PTI gene expression **(Fig. 2C)**. The induction
351 of BIR1 protein in the BIR1 L6 and L9 plants used for ROS and ethylene assays was confirmed
352 by immunocapture followed by western blot, while BIR1 transcript levels were monitored in
353 the samples used for RT-qPCR expression assays (**Fig. 2D**).

354 Collectively, these results indicate that BIR1 induction within a physiological threshold
355 has negligible effects on ROS production or ethylene accumulation but interferes with
356 downstream events in the PTI pathway leading to transcriptional activation of defense genes.

357

358 **Induction of BIR1 hinders callose deposition at PD triggered by flg22 or dsRNA**

359 Callose-containing depositions at the cell-wall and PD triggered by conserved PAMPs occur
360 during the early stages of pathogen invasion (Luna *et al.*, 2011). Deposition of callose at PD
361 regulates symplastic transport, and limits the ability of the invading pathogen to enter plant
362 tissues (De Storme & Geelen, 2014; Xu *et al.*, 2017; Huang *et al.*, 2023). To investigate whether
363 physiological induction of BIR1 could affect PD callose deposition, we used *in vivo* aniline
364 blue staining to quantify PD-associated callose from digital photographs of BIR1 L9
365 Arabidopsis plants. BIR1 was induced with a 30 µM DEX solution 3 times at 24h intervals,
366 whereas control plants were mock-treated with H_2O. We first investigated callose deposition
367 using 1 µM flg22 as elicitor. Flg22 treatment of control (DEX-) BIR1 L9 plants caused a
368 noticeable increase in PD callose intensity compared to plants treated without elicitor (H_2O)
369 **(Figs. 3A, C)**. In contrast, PD-associated callose induced by flg22 remained at H_2O-induced
370 control levels in BIR1-expressing plants (DEX+) **(Figs. 3A, C)**, indicating that BIR1 was able
371 to interfere, at least partially, with PD callose deposition triggered by flg22.

372 To study if BIR1-mediated callose inhibition was a general response, BIR1 L9 plants were
373 treated with the synthetic dsRNA analog polyinosinic-polycytidilic acid [poly(I:C)] (0.5 µg μl^{-}
374 ^{1}) since dsRNA is known to trigger deposition of callose and PD closure in Arabidopsis (Huang
375 *et al.*, 2023). In the absence of DEX, callose intensity was significantly higher in BIR1 L9
376 plants treated with poly(I:C) compared to H_2O-treated plants. In contrast, after DEX treatment,
377 poly(I:C)-induced callose was significantly repressed by the expression of BIR1 (**Figs. 3B, C**).
378 Callose was enhanced in DEX-treated WT plants in response to poly(I:C) relative to H_2O-
379 treated plants, suggesting that DEX does not affect callose deposition in the WT genotype **(Fig.
380 3C)**. These findings indicate that the activation of BIR1 impairs PD callose deposition induced
381 by different PAMP elicitors.

382 We further explored if callose accumulation elicited by poly(I:C) or flg22 at the PD was
383 SOBIR1-dependent using a *sobir1-12* mutant (Gao *et al.*, 2009; Liu *et al.*, 2016). We observed
384 enhanced callose deposition in WT plants in response to poly(I:C), whereas the median PD
385 callose level detected in *sobir1-12* plants after poly(I:C) treatment was similar to those triggered
386 in H_2O-treated *sobir1-12* plants **(Fig. 3D)**. Surprisingly, PD callose deposition in the *sobir1-12*
387 background was also reduced in response to flg22 (**Fig. 3D**). Callose activation at PD by both
388 elicitors was inhibited in the double *bir1-1 sobir1-1* mutant **(Fig. 3D).** These findings indicate
389 that callose deposition triggered by either dsRNA or bacterial flg22 involved the SOBIR1 co-
390 receptor.

391

392 **BIR1 overexpression triggers the expression of immunity-related genes**

393 To independently validate the RNA-Seq results, we used RT-qPCR to examine the expression
394 of a subset of DEGs using independent sets (not used for RNA-seq) of mock- and DEX-treated
395 BIR1 L9 plants collected after 12 days of treatment. Our results indicated that expression of
396 BIR1, PR1, RESPIRATORY BURST OXIDASE HOMOLOG PROTEIN D (RBOHD), FRK1
397 and CYTOCHROME P450 MONOOXYGENASE 79B2 (CYP79B2) defense genes were all
398 significantly up-regulated in Arabidopsis plants overexpressing BIR1 compared to mock-
399 treated controls, which is in good consistency with their RNA-Seq-based expression profiles
400 **(Fig. 4A)**.

401 A detailed inspection of the RNA-Seq data revealed that multiple genes involved in the
402 perception of pathogens and the activation of downstream defense pathways were misregulated
403 when BIR1 was overexpressed. To increase accuracy, in the following analyses we have
404 considered solely DEGs with a $|\log_2 (\text{Fold-Change})| \geq 1$ and adjusted p-value ≤ 0.01. Genes
405 encoding LRR-type RLKs in the Arabidopsis genome were significantly enriched in response
406 to high levels of BIR1 [n= 225, two-tailed Fisher's exact test, P = 0.001 (DeL9_12 vs
407 DeWT_12) and P=4.5E-4 (DeL9_12 vs MoL9_12)] **(Table S7)**. Besides, cysteine-rich RLKs
408 (CRK), which contain cysteine-rich repeats in their extracellular domain, were highly
409 overrepresented in the pool of DEGs [n= 42, two-tailed Fisher's exact test, P = 1.06E-6
410 (DeL9_12 vs DeWT_12) and P=1.86E-9 (DeL9_12 vs MoL9_12)] **(Table S7) (Fig. S4)** (Chen,
411 2001). CRKs are important in the perception of apoplastic ROS and, likely in association with
412 BAK1, in the activation of PTI, enhanced pathogen resistance and hypersensitive response-
413 associated cell death (Yeh *et al.*, 2015; Quezada *et al.*, 2019; Castro *et al.*, 2021). Furthermore,

414 we observed a high percentage of RLP coding genes in Arabidopsis, not expected by chance,
415 in the list of DEGs [n=57, two-tailed Fisher's exact test, P = 4.08E-5 (DeL9_12 vs DeWT_12)
416 and P=6.04E-9 (DeL9_12 vs MoL9_12)] **(Table S7) (Fig. S5)** (Wang *et al.*, 2008; Lv *et al.*,
417 2016). Most of LRR-RLK, CRK and RLP transcripts were up-regulated in response to elevated
418 BIR1, but not in DEX-treated WT plants. RNA-Seq data revealed that BIR1 overexpression
419 boosted the transcription of many other genes involved in PTI and ETI signaling **(Figs. 4B,**
420 **S6A)**. This includes the RLK co-receptors BAK1 and SOBIR1, RLCKs such as BIK1 and
421 several AvrPphB SUSCEPTIBLE1(PBS1)-LIKE (PBL) (PBL4, PBL12, PBL20) (Liang &
422 Zhou, 2018; Rao *et al.*, 2018) **(Table S7)**. Active BIK1 positively regulates a Ca^{2+} influx from
423 apoplast to cytosol that induces a conformational change in CPKs that switches on their kinase
424 activity (Li *et al.*, 2014; Yip Delormel & Boudsocq, 2019). Collectively, CPKs were not
425 differentially regulated in plants overexpressing BIR1, but many individual CPKs were
426 regarded as DEGs in our assay. For instance, the expression of CPK4-6 and CPK11, which are
427 key players for transcriptional reprogramming upon elicitor perception, was enhanced only in
428 DEX-treated BIR1 L9 plants **(Fig. S6B)** (Boudsocq *et al.*, 2010). Upon ligand perception, BIK1
429 dissociates from activated receptor complexes and phosphorylates the plasma membrane
430 NADPH oxidase RBOHD to generate extracellular ROS (Kadota *et al.*, 2014; Li *et al.*, 2014;
431 Marcec & Tanaka, 2021). Interestingly, RBOHD was induced in DEX-treated BIR1 L9 plants
432 after both 4 and 12 days of treatment, but not in their corresponding controls **(Figs. 4A, 4B)**.
433 We found that elevated BIR1 levels strongly increased the transcript abundance of genes
434 encoding the lipase-like proteins EDS1, PHYTOALEXIN DEFICIENT 4 (PAD4), and
435 SENESCENCE ASSOCIATED-GENE 101 (SAG101) as well as ACTIVATED DISEASE
436 RESISTANCE 1 (ADR1), which are required for TNL-receptor function during ETI **(Figs. 4B)**
437 (Zhou & Zhang, 2020; Ngou *et al.*, 2021; Pruitt *et al.*, 2021b; Sun *et al.*, 2021; Tian *et al.*,
438 2021). Accordingly, a large number of DEGs in our assay were annotated as disease resistance
439 (R) protein-coding genes, of which the TNL class was particularly enriched [n=100, two-tailed
440 Fisher's exact test, P = 0.06 (DeL9_12 vs DeWT_12) and P=4.4E-5 (DeL9_12 vs MoL9_12)]
441 (Swiderski *et al.*, 2009) **(Table S7)**. Conversely, neither NON-RACE SPECIFIC DISEASE
442 RESISTANCE 1 (NDR1) nor genes encoding CNL intracellular receptors, which require
443 NDR1, were differentially expressed in response to BIR1 overexpression **(Fig. 4B) (Table S3)**.
444 EDS5, which transduces downstream of SA in Arabidopsis (Nawrath *et al.*, 2002), was highly
445 up-regulated in a BIR1-dependent manner. Interestingly, BIR2 was distinctively up-regulated
446 in DEX-treated BIR1 L9 samples, whereas BIR3 and its partner CONSTITUTIVE SHADE
447 AVOIDANCE 1 (CSA1), which also interacts with BIR1, were unaffected in plants

448 overexpressing BIR1 **(Fig. S6A)** (Schulze *et al.*, 2022). Consistent with transcript levels,
449 SOBIR1, PAD4-dependent PR1 and EDS1 proteins were strongly up-regulated by BIR1
450 overexpression in DEX-treated BIR1 L9 plants, compared to the non-treated controls (**Figs.**
451 **4C, 5C**).

452 In conclusion, our data indicated that the overexpression of BIR1 significantly alters hormone
453 homeostasis and up-regulates multiple immune receptors and co-receptors involved in the
454 perception and signaling of ligands and effectors. Defense activation in BIR1 overexpressing
455 plants occurs in the absence of microbes or microbe-derived elicitors/effectors, and correlates
456 with growth phenotypes and cell death that are reminiscent of plants with constitutively
457 activated defenses (Lorrain *et al.*, 2003; Guzman-Benito *et al.*, 2019).

458

459 **Genetic disruption of SOBIR1, but not BAK1, partially rescues BIR1 overexpression**
460 **phenotypes**

461 SOBIR1 and BAK1 are necessary for activating cell death and constitutive defense responses
462 in the knock-out *bir1-1* mutant (Gao *et al.*, 2009; Liu *et al.*, 2016). Therefore, we tested if
463 SOBIR1 and BAK1 were also required for the phenotypes associated with non-physiological
464 doses of BIR1. A DEX-inducible BIR1-mCherry system was used to generate independent
465 homozygous transgenic lines in the well-characterized *sobir1-12* and *bak1-5* mutant
466 backgrounds (Gao *et al.*, 2009; Schwessinger *et al.*, 2011). Transgenic plants were sprayed with
467 30 µM DEX solution or H_2O (mock-treated controls) for 12 days at 24 h intervals to promote
468 BIR1 overexpression.

469 As previously shown, our reference set of DEX-treated BIR1 L9 plants accumulated high levels
470 of BIR1 transcripts, and displayed a range of stunting symptoms, accelerated senescence
471 (yellowing), and cell death relative to non-treated BIR1 L9 controls or DEX-treated WT plants
472 **(Fig. 5A)** (Guzman-Benito *et al.*, 2019). Nonetheless, growth retardation in DEX-treated plants
473 was partially due to DEX effects as shown for WT plants after 12 days of DEX treatment **(Fig.**
474 **5A)**. When *sobir1-12* BIR1 plants were investigated, we observed that the phenotypes after 12
475 days of DEX treatments, albeit variable between biological replicates, were milder than those
476 in BIR1 L9 plants, and ranged from typical WT appearance to localized yellowing and,
477 occasionally, discrete leaf necrosis **(Figs. 5A, S7A, S7B)**. Interestingly, BIR1 transcript and
478 protein accumulated in *sobir1-12* BIR1 plants like in BIR1 L9 plants after 12 days of DEX
479 application, discarding potential dose effects **(Fig. 5B, C)**. Furthermore, transcripts of the PTI-

480 markers RBOHD, FRK1 and WRKY DNA-BINDING PROTEIN 29 (WRK29) in DEX-treated
481 *sobir1-12* BIR1 plants, although slightly increased, were statistically indistinguishable from
482 non-treated controls **(Figs. 5D, S7C)**, suggesting that the up-regulation of PTI genes due to
483 BIR1 overexpression was affected by the lack of SOBIR1.

484 *bak1*-5 BIR1 plants consistently developed strong morphological phenotypes after 12 days of
485 DEX application, that closely resemble those of BIR1 L9 plants **(Figs. 5A, S7A, S7B)**. RT-
486 qPCR showed that BIR1 transcripts also accumulated in these plants after long DEX treatments,
487 although to a variable degree depending on the transgenic lines and biological replicates. For
488 instance, BIR1 transcript levels in *bak1*-5 BIR1 plants were comparable to those in *sobir1-12*
489 BIR1 plants in **Fig. S7B**. Besides, differences in BIR1 protein accumulation were observed
490 between DEX-treated *bak1-5* BIR1 L4 and L10 lines in this experiment **(Fig. 5C)**. Conversely,
491 **Figs. 5A** and **B** illustrate data from a different experimental replicate in which BIR1 transcripts
492 in *bak1*-5 BIR1 plants were much less abundant than in BIR1 L9 plants. These interesting
493 observations suggest that the persistent induction of BIR1 over time, rather than an excess of
494 BIR1, was the trigger of the morphological alterations in the *bak1*-5 mutant background.
495 RBOHD, FRK1 and WRKY remained transcriptionally up-regulated in DEX-treated *bak1-5*
496 BIR1 plants as they did in BIR1 L9 plants **(Figs. 5E)**. Collectively, these data indicate that the
497 morphological phenotypes and the activation of PTI defense genes that occur when BIR1 is
498 continually induced or overexpressed were partially dependent on SOBIR1, but genetically
499 unrelated to BAK1.

500 Alterations in plant hormone pathways may negatively affect plant growth (Denance *et al.*,
501 2013). The transcriptional reprogramming of genes involved in plant hormone metabolism and
502 signaling in BIR1-overexpressing plants prompted us to further examine their expression in the
503 mutant backgrounds mentioned above. RT-qPCR revealed that genes encoding salicylic acid
504 (SA)-dependent PR1, jasmonic acid (JA)-responsive PLANT DEFENSIN 1.2 (PDF1.2),
505 ethylene (ET)- and JA-responsive PR4 as well as genes encoding the cytochrome P450 enzymes
506 CYP71B15 (PAD3) and CYP79B2 involved in camalexin (CA)-biosynthesis and CA-mediated
507 plant defense, were all up-regulated in BIR1-overexpressing plants of *sobir1-12* BIR1
508 genotypes **(Fig. 5F)**. Intriguingly, the induction of these genes was notably reduced in *bak1-5*
509 BIR1 plants after DEX treatment compared to *sobir1-12* BIR1 or BIR1 L9 plants **(Fig. 4A,**
510 **5G)**. This data suggests that the *bak1-5* mutation may compromise, at least partially, defense
511 hormone signaling upon BIR1 overexpression. None of these genes, except PR1, were induced

512 or repressed in DEX-treated WT plants, discarding a potential effect of DEX on their expression
513 **(Table S3)**.

514

515 **Genetic disruption of EDS1, but not PAD4, partially rescues BIR1 overexpression**
516 **phenotypes**

517 A previous report showed that growth stunting, activation of cell death and defense responses
518 in the *bir1-1* mutant are partially dependent on EDS1 and PAD4 (Gao *et al.*, 2009). The EDS1-
519 PAD4 node has a relevant role in PRR signaling and TNL activation, indicating that it mediates
520 both PTI and ETI (Pruitt *et al.*, 2021a). Given that TNL-coding transcripts were abundant in
521 BIR1 L9 plants and that EDS1 transcripts and protein were elevated in BIR1 L9, *sobir1-12*
522 BIR1 and *bak1-5* BIR1 plants (**Figs. 5B, C**), we wondered if TNL-mediated ETI responses
523 along with, or independently of, PTI could be important for BIR1 overexpression phenotypes.
524 Thus, we tested if the phenotypes caused by sustained BIR1 induction were dependent on EDS1
525 or PAD4. The DEX-inducible BIR1-mCherry system was used to generate homozygous
526 transgenic lines from *eds1-2* and *pad4-1* mutants (Parker *et al.*, 1996; Zhou *et al.*, 1998). The
527 *eds1-2* BIR1 plants presented mostly WT-like morphologies and, occasionally, localized
528 yellowing after 12 days of DEX treatments compared to non-treated plants **(Figs. 6A, S7A)**.
529 Importantly, RT-qPCR analysis showed that BIR1 accumulated in the *eds1-2* BIR1 plants as
530 much as in the BIR1 L9 plants **(Figs. 6A)**. The expression of FRK1 and RBOHD was
531 significantly enhanced in *eds1-2* BIR1 plants after DEX applications compared to non-treated
532 controls **(Fig. 6B)**. Our data indicate that the lack of EDS1 attenuates the morphological
533 phenotypes caused by BIR1 overexpression, and pose the possibility that these phenotypic
534 alterations and the activation of PTI genes are unconnected processes.

535 Next, we found that *pad4-1* BIR1 plants had essentially BIR1 L9-like phenotypes after 12 days
536 of DEX applications **(Figs. 6A, S7A)**. In these plants, BIR1 accumulated much less than in
537 BIR1 L9 or *eds1-2* BIR1 plants **(Fig. 6A)**. As shown for *bak1-5* BIR1 plants, we presume that
538 sustained BIR1 induction, rather than BIR1 overexpression, was sufficient to cause typical
539 BIR1 phenotypes regardless of the *pad4-1* mutation. Interestingly, PTI-components FRK1,
540 WRKY29 and RBOHD showed no responsiveness to BIR1 overexpression in *pad4-1* BIR1
541 plants, which support the idea that cell death and PTI activation are unrelated in these plants
542 **(Figs. 6C, S7C)**. In summary, we observed that the genetic elimination of EDS1, but not PAD4,
543 contributes to mitigating the morphological phenotypes caused by continuous BIR1

544 induction/overexpression, and suggests that symptoms arise from the activation of EDS1-
545 dependent ETI-type cell death rather than the disruption of PRR-mediated PTI responses.

546 RT-qPCR revealed a significant transcriptional activation of marker genes in the SA, JA, ET
547 and CA pathways in response to high levels of BIR1 in DEX-treated *eds1-2* BIR1 plants versus
548 non-treated controls **(Fig. 6D)**. On the contrary, the same markers were poorly or no longer up-
549 regulated in *pad4*-1 BIR1 transgenics after 12 days of DEX treatments relative to the non-
550 treated controls, suggesting that PAD4 is important for PTI gene expression and phytohormone
551 homeostasis **(Fig. 6E)**.

552

553 **Phenotypes of BIR1 overexpressing lines are unrelated to SA signaling pathways**

554 Previously, high SA levels were found as partly responsible for *bir1-1* phenotypes (Gao *et al.*,
555 2009). However, *pad4-1* BIR1 plants were as sensitive as BIR1 L9 plants to DEX treatments,
556 suggesting that morphological phenotypes caused by non-physiological BIR1 levels are
557 independent of SA-mediated signaling. To confirm this prediction, the effects of mutations in
558 the SA biosynthesis on the growth and defense activation in BIR1 overexpressing plants were
559 assessed. In Arabidopsis, SALICYLIC ACID INDUCTION DEFICIENT
560 2/ISOCHORISMATE SYNTHASE 1 (SID2/ICS1) and EDS5 are involved in pathogen-
561 induced SA biosynthesis (Huang *et al.*, 2020). Therefore, DEX-inducible BIR1-mCherry
562 transgenics were generated in the *sid2-2* and *eds5-3* genetic backgrounds. We found that *sid2-*
563 *2* BIR1 plants exhibited from moderate to severe morphological phenotypes after 12 days of
564 DEX treatment that coincided with moderate levels of BIR1 overexpression relative to those
565 observed in BIR1 L9 plants **(Figs. 7A, B)**. *eds5*-3 BIR1 plants typically displayed strong
566 developmental defects and necrosis and accumulated BIR1 transcripts at BIR1 L9 levels after
567 long DEX applications **(Figs. 7A, C)**. The transcription levels of PDF1.2 and CYP79B2, but
568 not PAD3, were high in DEX-treated *sid2*-2 BIR1 plants compared to non-treated controls **(Fig.**
569 **7B)**, while PAD3 and PDF1.2, but not CYP79B2 were up-regulated in *eds5-3* BIR1
570 overexpressing plants relative to non-treated controls **(Fig. 7C)**. Our findings confirm that the
571 phenotypical alterations linked to BIR1 overexpression were not drastically affected by
572 disruptive mutations in SA biosynthesis (*sid2-2* and *eds5-3*) and SA signaling (*pad4-1*).

573

574 **Discussion**

575 Plants respond to microbes and viruses by enhancing the expression of multiple genes that
576 function as regulators or executors of various defense programs (Nishad *et al.*, 2020). Among
577 them, BIR1 was shown to be up-regulated during bacterial and oomycete infections, and during
578 viral infections in a SA-dependent manner (Gao *et al.*, 2009; Guzman-Benito *et al.*, 2019). The
579 observation that knock-out *bir1-1* mutants have increased resistance to the virulent oomycete
580 *Hyaloperonospora parasitica* Noco2 and to the RNA virus *Tobacco rattle virus* (TRV) suggests
581 an active role in plant immunity (Gao *et al.*, 2009; Guzman-Benito *et al.*, 2019). Since BIR1 is
582 a negative regulator of cell death and defense (Liu *et al.*, 2016; Ma *et al.*, 2017), we
583 hypothesized that BIR1 induction might be part of a common strategy to modulate, at least
584 partially, the amplitude of the immune responses during microbial and viral infections. To test
585 the hypothesis, we used a previously described DEX-inducible system for the conditional
586 expression of a mCherry-tagged BIR1 transgene in Arabidopsis (Guzman-Benito *et al.*, 2019).
587 This system allowed us to investigate the outputs associated with short and long BIR1 induction
588 times. Importantly, BIR1 induction is triggered in the absence of immune elicitors or effectors
589 that could otherwise initiate undesirable localized and systemic defense responses in the plant.
590 Upon short-term DEX treatments, BIR1 accumulates in rosette leaves to levels comparable to
591 those observed under natural conditions in bacteria- or virus-infected plants, or plants treated
592 with SA (Gao *et al.*, 2009; Guzman-Benito *et al.*, 2019). In the absence of pathogens or elicitors,
593 short induction of BIR1 has a subtle, if any, impact on both plant transcriptome and plant
594 morphology. In contrast, in the presence of the PTI elicitor flg22, the physiological induction
595 of BIR1 negatively affects the expression of several PTI-marker genes, whereas it has no effects
596 on ROS burst, as previously shown (Liu *et al.*, 2016), or production of ethylene. This
597 observation suggests that BIR1 can regulate, directly or indirectly, the activity of components
598 in the PTI signaling pathway that ultimately control immune gene transcription. Likewise, BIR1
599 activation compromises the callose deposition at PD elicited by either flg22 or the dsRNA-
600 analog poly(I:C). PD allow cell-to-cell and long-distance transport of micro- and
601 macromolecules, representing gateways through which plant viruses pass from cell to cell to
602 spread infections (De Storme & Geelen, 2014). Targeted deposition of callose modulates
603 symplastic connectivity by regulating PD pore size, and therefore constitutes an essential layer
604 in the defense against pathogens (Wang *et al.*, 2021). According to our data, induction of BIR1
605 during pathogen attack can be interpreted as a strategy to regulate PD trafficking. Although not
606 tested in this study, BIR1 effects on gene expression and callose deposition may render PTI less
607 effective against pathogens. Indeed, PTI gene expression and callose formation are usually
608 blocked/inhibited by many defense-suppressing virulence effectors from different types of

609 microbes (Cui *et al.*, 2009; Wang *et al.*, 2021). Viral-encoded proteins such as the potyviral
610 silencing suppressor helper-component proteinase (HC-Pro) or the movement protein (MP) of
611 several tobamoviruses are capable of suppressing callose deposition (Citovsky *et al.*, 1990;
612 Chowdhury *et al.*, 2020). A recent work shows that tobamovirus MPs promote viral cell-to-cell
613 propagation by blocking dsRNA-induced callose deposition (Huang *et al.*, 2023). It is tempting
614 to speculate that BIR1 induction during the viral infection controls PD callose deposition, and
615 perhaps other antiviral defenses, triggered by viral-derived dsRNA. dsRNA-induced deposition
616 of callose requires PTI signaling components such as SERK1 and BIK1/PBL1 (Huang *et al.*,
617 2023). Our results show that PD callose deposition elicited by flg22 or poly(I:C) is inhibited in
618 the *sobir1-1* mutant. This observation is puzzling because flg22 signaling is independent of
619 SOBIR1. Further research is needed to understand the role of SOBIR1 in controlling PD callose
620 deposition.

621 Long DEX treatments of BIR1 transgenic plants led to sustained and/or elevated BIR1 levels
622 (non-physiological) similar to those expected if BIR1 gene regulation were lost. Under these
623 conditions, plants exhibit dramatic changes in gene expression and eventually strong
624 morphological and growth phenotypes, including accelerated senescence (yellowing), stunting,
625 necrosis and cell death (Guzman-Benito *et al.*, 2019). An excess of BIR1 in our transgenic
626 plants also induced the activation of multiple genes involved in different branches of the PTI
627 and ETI signaling responses. Among them, the up-regulation of a significant number of RLP-
628 coding genes is striking. RLPs have been observed predominantly expressed in senescence
629 leaves, supporting the idea that BIR1 overexpression accelerates a senescence program (Wang
630 *et al.*, 2008). In Arabidopsis, RLP1, RLP23, RLP30, RLP32 and RLP42 mediate SOBIR1-
631 dependent immune activation, but the role of most RLPs in the perception of pathogen and
632 defense is unknown (Wang *et al.*, 2008; Zhang *et al.*, 2013; Albert *et al.*, 2019). The
633 overexpression of genes encoding TNL-resistance proteins, but not CNLs, is another important
634 feature linked to high levels of BIR1. Here, we provide genetic evidence that morphological
635 phenotypes due to sustained BIR1 induction are partially dependent on EDS1. TNL-based
636 immunity is mediated by two distinct signaling modules, EDS1/SAG101/NRG1 and
637 EDS1/PAD4/ADR1 (Sun *et al.*, 2021). Since knocking out PAD4 had little influence on BIR1
638 overexpression phenotypes, we propose that EDS1, perhaps in concert with SAG101, triggers
639 cell death-like phenotypes upon TNL activation in BIR1 overexpressing plants **(Fig. 7D)**. How
640 TNL receptors are activated when BIR1 is strongly expressed is a question to resolve. A current
641 model postulates that loss of BIR1 function leads to the activation of hypothetical guarding R

642 proteins which further feed PAD4- and SOBIR1-dependent resistance pathways (Gao *et al.*,
643 2009). Our results are also coherent with BIR1 or a yet unknown BIR1/SERK complex being
644 guarded by one or several EDS1-dependent TNL proteins. Therefore, non-physiological
645 induction of BIR1 may promote TNL-mediated resistance pathways that require EDS1 when
646 no effectors or elicitors are present. In addition to EDS1, we demonstrated that SOBIR1 is
647 necessary for BIR1 overexpression phenotypes. The role of SOBIR1 in the BIR1 pathway is
648 unclear. Although extensive investigation is required, SOBIR1 may function as a specific co-
649 regulator of the EDS1-dependent responses triggered by BIR1 overexpression, as part of the
650 same signaling pathway **(Fig. 7D)**. This idea is inspired by a recent work showing that the cell-
651 surface RLP23 receptor uses SOBIR1 to form a supramolecular complex with a
652 EDS1/PAD4/ADR1 node in a ligand-independent manner to mediate defense signaling
653 cascades that are common to both surface PRR (PTI) and NLR (ETI) receptors (Pruitt *et al.*,
654 2021b). The TNL protein CSA1 senses perturbances of BIR3, BAK1 or BIR3/BAK1
655 complexes leading to ETI-type autoimmune responses (Schulze *et al.*, 2022). CSA1 did not
656 show responsiveness to BIR1 overexpression in our assay, but it has been shown to interact
657 with BIR1 (Schulze *et al.*, 2022). It will be interesting to see if CSA1 also guards BIR1 integrity,
658 perhaps in cooperation with SOBIR1 and/or other SERKs **(Fig. 7D)**. Finally, phenotypes linked
659 to BIR1 overexpression were apparently unaffected by the *bak1-5* mutation, which suggests
660 that other SERK family members can compensate for the loss of BAK1 in PTI/ETI signaling.

661 We observed that the up-regulation of FRK1, WRKY29 and RBOHD due to BIR1
662 overexpression was compromised by mutations in SOBIR1 and PAD4, but it was independent
663 of EDS1. Since EDS1, PAD4 and SOBIR1 are important for both cell surface PRR receptor-
664 and TNL-mediated signaling and resistance (Pruitt *et al.*, 2021b; Tian *et al.*, 2021), we will
665 need additional experimentation to establish if changes in PTI gene expression involve PTI-
666 dependent pathways, TNL activation or other unknown mechanisms yet to be determined. Our
667 study also revealed significant alterations in plant hormone gene expression. Interestingly,
668 genes related to the plant hormones ET, JA, CA, and SA, which play a central role in regulating
669 immune responses, remained up-regulated in *eds1-2* BIR1 and *sobir1-12* BIR1 backgrounds,
670 in which phenotypes were partially rescued. This suggests that i) regulation of hormone
671 homeostasis does not require SOBIR1- and/or EDS1-mediated signaling pathways, and that ii)
672 such hormonal imbalance has little, if any, influence on the ETI-like phenotypes observed in
673 BIR1 overexpressing plants.

674

675 **Conclusions**

676 Here, we investigated the implications of BIR1 homeostasis on the immune response in
677 Arabidopsis. BIR1 induction at physiological levels interferes with both immune gene
678 expression and PD callose deposition triggered by canonical PTI elicitors. We posit that BIR1
679 induction may represent a pathogen-driven mechanism to modulate plant defenses, and that this
680 mechanism helps to maintain a host-pathogen equilibrium during infections. Over time
681 induction of BIR1 typically leads to high levels on BIR1 in the plant tissue, and causes severe
682 morphological and growth defects concomitant with transcriptomic changes affecting plant
683 immunity. These findings indicate a dose-dependency of the BIR1 regulatory activity, in which
684 BIR1 induction/BIR1 overexpression over time results in autoimmunity and fitness penalties.
685 We provide experimental evidence that both EDS1 and SOBIR1, but neither PAD4 nor BAK1,
686 were necessary for the ETI-type cell death phenotypes that occur when BIR1 is overexpressed.
687 We hypothesize that one or several unknown TNLs monitor the integrity of BIR1 or BIR1-co-
688 receptor complexes and that SOBIR1 cooperates with EDS1 to transduce signals downstream
689 of TNL **(Fig. 7D)**.

690

691 **Acknowledgements**

692 This work was supported by National Research grants RTI2018-096979-B-I00 and PID2021
693 7982NB-I00 to CL from Ministerio de Ciencia e Innovación (Spain) and UE-FEDER, and grant
694 iLINKA20415 to CL from CSIC (Spain). Contributions of ARS, LEG and MH were supported
695 by grants ERA-NET SusCrop2 / ANR-21-SUSC-0003-01 and ANR-PRC / ANR-21-CE20-
696 0020-01 to MH. We thank Rosa Lozano-Durán, Birgit Kemmerling, Laura Medina-Puche and
697 Delphine Pott for critical reading and colleagues who kindly donated seeds and materials.

698

699 **Author contributions**

700 CL and IGB conceived and designed the study. CL, IGB, CR and IP performed expression
701 assays and transgenics. CL and CH performed ROS and ethylene assays. CL, ARS and LEG
702 performed callose assays. CL, IGB, MH and TN analyzed the data. CL wrote the article.

703

704 **REFERENCES**

705 **Albert I, Bohm H, Albert M, Feiler CE, Imkampe J, Wallmeroth N, Brancato C,**
706 **Raaymakers TM, Oome S, Zhang H, et al. 2015.** An RLP23-SOBIR1-BAK1 complex
707 mediates NLP-triggered immunity. *Nat Plants* **1**: 15140.
708 **Albert I, Zhang L, Bemm H, Nurnberger T. 2019.** Structure-function analysis of immune
709 receptor AtRLP23 with its ligand nlp20 and coreceptors AtSOBIR1 and AtBAK1. *Mol*
710 *Plant Microbe Interact* **32**(8): 1038-1046.
711 **Belkhadir Y, Jaillais Y, Epple P, Balsemao-Pires E, Dangl JL, Chory J. 2012.**
712 Brassinosteroids modulate the efficiency of plant immune responses to microbe-associated
713 molecular patterns. *Proc Natl Acad Sci U S A* **109**(1): 297-302.
714 **Bi G, Zhou Z, Wang W, Li L, Rao S, Wu Y, Zhang X, Menke FLH, Chen S, Zhou JM.**
715 **2018.** Receptor-like cytoplasmic kinases directly link diverse pattern recognition Receptors
716 to the activation of mitogen-activated protein kinase cascades in Arabidopsis. *Plant Cell*
717 **30**(7): 1543-1561.
718 **Boudsocq M, Willmann MR, McCormack M, Lee H, Shan L, He P, Bush J, Cheng SH,**
719 **Sheen J. 2010.** Differential innate immune signalling via Ca(2+) sensor protein kinases.
720 *Nature* **464**(7287): 418-422.
721 **Boutrot F, Zipfel C. 2017.** Function, discovery, and exploitation of plant pattern recognition
722 receptors for broad-spectrum disease resistance. *Annu Rev Phytopathol* **55**: 257-286.
723 **Castro B, Citterico M, Kimura S, Stevens DM, Wrzaczek M, Coaker G. 2021.** Stress-
724 induced reactive oxygen species compartmentalization, perception and signalling. *Nat*
725 *Plants* **7**(4): 403-412.
726 **Chen Z. 2001.** A superfamily of proteins with novel cysteine-rich repeats. *Plant Physiol* **126**(2):
727 473-476.
728 **Chowdhury RN, Lasky D, Karki H, Zhang Z, Goyer A, Halterman D, Rakotondrafara**
729 **AM. 2020.** HCPro suppression of callose deposition contributes to strain-specific
730 resistance against Potato Virus Y. *Phytopathology* **110**(1): 164-173.
731 **Citovsky V, Knorr D, Schuster G, Zambryski P. 1990.** The P30 movement protein of tobacco
732 mosaic virus is a single-strand nucleic acid binding protein. *Cell* **60**(4): 637-647.
733 **Clough SJ, Bent AF. 1998.** Floral dip: a simplified method for Agrobacterium-mediated
734 transformation of Arabidopsis thaliana. *Plant J* **16**(6): 735-743.
735 **Couto D, Zipfel C. 2016.** Regulation of pattern recognition receptor signalling in plants. *Nat*
736 *Rev Immunol* **16**(9): 537-552.
737 **Cui H, Xiang T, Zhou JM. 2009.** Plant immunity: a lesson from pathogenic bacterial effector
738 proteins. *Cell Microbiol* **11**(10): 1453-1461.

739 **De Storme N, Geelen D. 2014.** Callose homeostasis at plasmodesmata: molecular regulators
740 and developmental relevance. *Front Plant Sci* **5**: 138.
741 **Denance N, Sanchez-Vallet A, Goffner D, Molina A. 2013.** Disease resistance or growth: the
742 role of plant hormones in balancing immune responses and fitness costs. *Front Plant Sci*
743 **4**: 155.
744 **Dominguez-Ferreras A, Kiss-Papp M, Jehle AK, Felix G, Chinchilla D. 2015.** An overdose
745 of the Arabidopsis coreceptor BRASSINOSTEROID INSENSITIVE1-ASSOCIATED
746 RECEPTOR KINASE1 or its ectodomain causes autoimmunity in a SUPPRESSOR OF
747 BIR1-1-dependent manner. *Plant Physiol* **168**(3): 1106-1121.
748 **Fernandez-Calvino L, Guzman-Benito I, Del Toro FJ, Donaire L, Castro-Sanz AB, Ruiz-**
749 **Ferrer V, Llave C. 2016.** Activation of senescence-associated Dark-inducible (DIN) genes
750 during infection contributes to enhanced susceptibility to plant viruses. *Mol Plant Pathol*
751 **17**(1): 3-15.
752 **Gao M, Wang X, Wang D, Xu F, Ding X, Zhang Z, Bi D, Cheng YT, Chen S, Li X, et al.**
753 **2009.** Regulation of cell death and innate immunity by two receptor-like kinases in
754 Arabidopsis. *Cell Host Microbe* **6**(1): 34-44.
755 **Gust AA, Pruitt R, Nurnberger T. 2017.** Sensing danger: key to activating plant immunity.
756 *Trends Plant Sci* **22**(9): 779-791.
757 **Guzman-Benito I, Donaire L, Amorim-Silva V, Vallarino JG, Esteban A, Wierzbicki AT,**
758 **Ruiz-Ferrer V, Llave C. 2019.** The immune repressor BIR1 contributes to antiviral
759 defense and undergoes transcriptional and post-transcriptional regulation during viral
760 infections. *New Phytol* **224**(1): 421-438.
761 **Halter T, Imkampe J, Mazzotta S, Wierzba M, Postel S, Bucherl C, Kiefer C, Stahl M,**
762 **Chinchilla D, Wang X, et al. 2014.** The leucine-rich repeat receptor kinase BIR2 is a
763 negative regulator of BAK1 in plant immunity. *Curr Biol* **24**(2): 134-143.
764 **Hohmann U, Lau K, Hothorn M. 2017.** The structural basis of ligand perception and signal
765 activation by receptor kinases. *Annu Rev Plant Biol* **68**: 109-137.
766 **Huang C, Mutterer J, Heinlein M. 2022.** In vivo aniline blue staining and semiautomated
767 quantification of callose deposition at plasmodesmata. *Methods Mol Biol* **2457**: 151-165.
768 **Huang C, Sede AR, Elvira-González L, Yan Y, Rodriguez M, Mutterer J, Boutant E, Shan**
769 **L, Heinlein M. 2023.** dsRNA-induced immunity targets plasmodesmata and is suppressed
770 by viral movement proteins. *Plant Cell* https://doi.org/10.1101/2022.11.21.517408.
771 **Huang W, Wang Y, Li X, Zhang Y. 2020.** Biosynthesis and regulation of salicylic acid and
772 N-hydroxypipecolic acid in plant immunity. *Mol Plant* **13**(1): 31-41.

773 **Imkampe J, Halter T, Huang S, Schulze S, Mazzotta S, Schmidt N, Manstretta R, Postel**
774 **S, Wierzba M, Yang Y, et al. 2017.** The Arabidopsis leucine-rich repeat receptor kinase
775 BIR3 negatively regulates BAK1 receptor complex formation and stabilizes BAK1. *Plant*
776 *Cell* **29**(9): 2285-2303.
777 **Jubic LM, Saile S, Furzer OJ, El Kasmi F, Dangl JL. 2019.** Help wanted: helper NLRs and
778 plant immune responses. *Curr Opin Plant Biol* **50**: 82-94.
779 **Kadota Y, Sklenar J, Derbyshire P, Stransfeld L, Asai S, Ntoukakis V, Jones JD, Shirasu**
780 **K, Menke F, Jones A, et al. 2014.** Direct regulation of the NADPH oxidase RBOHD by
781 the PRR-associated kinase BIK1 during plant immunity. *Mol Cell* **54**(1): 43-55.
782 **Korner CJ, Klauser D, Niehl A, Dominguez-Ferreras A, Chinchilla D, Boller T, Heinlein**
783 **M, Hann DR. 2013.** The immunity regulator BAK1 contributes to resistance against
784 diverse RNA viruses. *Mol Plant Microbe Interact* **26**(11): 1271-1280.
785 **Lee DH, Lee HS, Belkhadir Y. 2021.** Coding of plant immune signals by surface receptors.
786 *Curr Opin Plant Biol* **62**: 102044.
787 **Li L, Li M, Yu L, Zhou Z, Liang X, Liu Z, Cai G, Gao L, Zhang X, Wang Y, et al. 2014.**
788 The FLS2-associated kinase BIK1 directly phosphorylates the NADPH oxidase RbohD to
789 control plant immunity. *Cell Host Microbe* **15**(3): 329-338.
790 **Li P, Lu YJ, Chen H, Day B. 2020.** The Lifecycle of the plant immune system. *CRC Crit Rev*
791 *Plant Sci* **39**(1): 72-100.
792 **Liang X, Zhou JM. 2018.** Receptor-like cytoplasmic kinases: central players in plant receptor
793 kinase-mediated signaling. *Annu Rev Plant Biol* **69**: 267-299.
794 **Liebrand TW, van den Burg HA, Joosten MH. 2014.** Two for all: receptor-associated kinases
795 SOBIR1 and BAK1. *Trends Plant Sci* **19**(2): 123-132.
796 **Liu Y, Huang X, Li M, He P, Zhang Y. 2016.** Loss-of-function of Arabidopsis receptor-like
797 kinase BIR1 activates cell death and defense responses mediated by BAK1 and SOBIR1.
798 *New Phytol* **212**(3): 637-645.
799 **Lorrain S, Vailleau F, Balague C, Roby D. 2003.** Lesion mimic mutants: keys for deciphering
800 cell death and defense pathways in plants? *Trends Plant Sci* **8**(6): 263-271.
801 **Luna E, Pastor V, Robert J, Flors V, Mauch-Mani B, Ton J. 2011.** Callose deposition: a
802 multifaceted plant defense response. *Mol Plant Microbe Interact* **24**(2): 183-193.
803 **Lv Y, Yang N, Wu J, Liu Z, Pan L, Lv S, Wang G. 2016.** New insights into receptor-like
804 protein functions in Arabidopsis. *Plant Signal Behav* **11**(7): e1197469.

805 **Ma C, Liu Y, Bai B, Han Z, Tang J, Zhang H, Yaghmaiean H, Zhang Y, Chai J. 2017.**
806 Structural basis for BIR1-mediated negative regulation of plant immunity. *Cell Res* **27**(12):
807 1521-1524.
808 **Macho AP, Lozano-Duran R. 2019.** Molecular dialogues between viruses and receptor-like
809 kinases in plants. *Mol Plant Pathol* **20**(9): 1191-1195.
810 **Marcec MJ, Tanaka K. 2021.** Crosstalk between calcium and ROS signaling during flg22-
811 triggered immune response in Arabidopsis leaves. *Plants (Basel)* **11**(1).
812 **McHale L, Tan X, Koehl P, Michelmore RW. 2006.** Plant NBS-LRR proteins: adaptable
813 guards. *Genome Biol* **7**(4): 212.
814 **Mithoe SC, Menke FL. 2018.** Regulation of pattern recognition receptor signalling by
815 phosphorylation and ubiquitination. *Curr Opin Plant Biol* **45**(Pt A): 162-170.
816 **Nawrath C, Heck S, Parinthawong N, Metraux JP. 2002.** EDS5, an essential component of
817 salicylic acid-dependent signaling for disease resistance in Arabidopsis, is a member of the
818 MATE transporter family. *Plant Cell* **14**(1): 275-286.
819 **Ngou BPM, Ahn HK, Ding P, Jones JDG. 2021.** Mutual potentiation of plant immunity by
820 cell-surface and intracellular receptors. *Nature* **592**(7852): 110-115.
821 **Ngou BPM, Ding P, Jones JDG. 2022.** Thirty years of resistance: Zig-zag through the plant
822 immune system. *Plant Cell* **34**(5): 1447-1478.
823 **Nishad R, Ahmed T, Rahman VJ, Kareem A. 2020.** Modulation of plant defense system in
824 response to microbial interactions. *Front Microbiol* **11**: 1298.
825 **Parker JE, Holub EB, Frost LN, Falk A, Gunn ND, Daniels MJ. 1996.** Characterization of
826 eds1, a mutation in Arabidopsis suppressing resistance to Peronospora parasitica specified
827 by several different RPP genes. *Plant Cell* **8**(11): 2033-2046.
828 **Pruitt RN, Gust AA, Nurnberger T. 2021a.** Plant immunity unified. *Nat Plants* **7**(4): 382-
829 383.
830 **Pruitt RN, Locci F, Wanke F, Zhang L, Saile SC, Joe A, Karelina D, Hua C, Frohlich K,**
831 **Wan WL, et al. 2021b.** The EDS1-PAD4-ADR1 node mediates Arabidopsis pattern-
832 triggered immunity. *Nature* **598**(7881): 495-499.
833 **Quezada EH, Garcia GX, Arthikala MK, Melappa G, Lara M, Nanjareddy K. 2019.**
834 Cysteine-rich receptor-like kinase gene family identification in the phaseolus genome and
835 comparative analysis of their expression profiles specific to mycorrhizal and rhizobial
836 symbiosis. *Genes (Basel)* **10**(1).

837 **Rao S, Zhou Z, Miao P, Bi G, Hu M, Wu Y, Feng F, Zhang X, Zhou JM. 2018.** Roles of
838 receptor-like cytoplasmic kinase VII members in pattern-triggered immune signaling.
839 *Plant Physiol* **177**(4): 1679-1690.
840 **Schulze S, Yu L, Hua C, Zhang L, Kolb D, Weber H, Ehinger A, Saile SC, Stahl M, Franz-**
841 **Wachtel M, et al. 2022.** The Arabidopsis TIR-NBS-LRR protein CSA1 guards BAK1-
842 BIR3 homeostasis and mediates convergence of pattern- and effector-induced immune
843 responses. *Cell Host Microbe* **30**(12): 1717-1731 e1716.
844 **Schwessinger B, Roux M, Kadota Y, Ntoukakis V, Sklenar J, Jones A, Zipfel C. 2011.**
845 Phosphorylation-dependent differential regulation of plant growth, cell death, and innate
846 immunity by the regulatory receptor-like kinase BAK1. *PLoS Genet* **7**(4): e1002046.
847 **Smakowska-Luzan E, Mott GA, Parys K, Stegmann M, Howton TC, Layeghifard M,**
848 **Neuhold J, Lehner A, Kong J, Grunwald K, et al. 2018.** An extracellular network of
849 Arabidopsis leucine-rich repeat receptor kinases. *Nature* **553**(7688): 342-346.
850 **Sun X, Lapin D, Feehan JM, Stolze SC, Kramer K, Dongus JA, Rzemieniewski J,**
851 **Blanvillain-Baufume S, Harzen A, Bautor J, et al. 2021.** Pathogen effector recognition-
852 dependent association of NRG1 with EDS1 and SAG101 in TNL receptor immunity. *Nat*
853 *Commun* **12**(1): 3335.
854 **Swiderski MR, Birker D, Jones JD. 2009.** The TIR domain of TIR-NB-LRR resistance
855 proteins is a signaling domain involved in cell death induction. *Mol Plant Microbe Interact*
856 **22**(2): 157-165.
857 **Tang D, Wang G, Zhou JM. 2017.** Receptor kinases in plant-pathogen interactions: more than
858 pattern recognition. *Plant Cell* **29**(4): 618-637.
859 **Tian H, Wu Z, Chen S, Ao K, Huang W, Yaghmaiean H, Sun T, Xu F, Zhang Y, Wang S,**
860 **et al. 2021.** Activation of TIR signalling boosts pattern-triggered immunity. *Nature*
861 **598**(7881): 500-503.
862 **van Wersch S, Tian L, Hoy R, Li X. 2020.** Plant NLRs: The whistleblowers of plant immunity.
863 *Plant Commun* **1**(1): 100016.
864 **Wan WL, Zhang L, Pruitt R, Zaidem M, Brugman R, Ma X, Krol E, Perraki A, Kilian J,**
865 **Grossmann G, et al. 2019.** Comparing Arabidopsis receptor kinase and receptor protein-
866 mediated immune signaling reveals BIK1-dependent differences. *New Phytol* **221**(4):
867 2080-2095.
868 **Wang G, Ellendorff U, Kemp B, Mansfield JW, Forsyth A, Mitchell K, Bastas K, Liu CM,**
869 **Woods-Tor A, Zipfel C, et al. 2008.** A genome-wide functional investigation into the
870 roles of receptor-like proteins in Arabidopsis. *Plant Physiol* **147**(2): 503-517.

871 **Wang J, Chai J. 2020.** Structural insights into the plant immune receptors PRRs and NLRs.
872 *Plant Physiol* **182**(4): 1566-1581.
873 **Wang Y, Li X, Fan B, Zhu C, Chen Z. 2021.** Regulation and function of defense-related
874 callose deposition in plants. *Int J Mol Sci* **22**(5).
875 **Withers J, Dong X. 2017.** Post-translational regulation of plant immunity. *Curr Opin Plant*
876 *Biol* **38**: 124-132.
877 **Wu Y, Gao Y, Zhan Y, Kui H, Liu H, Yan L, Kemmerling B, Zhou JM, He K, Li J. 2020.**
878 Loss of the common immune coreceptor BAK1 leads to NLR-dependent cell death. *Proc*
879 *Natl Acad Sci U S A* **117**(43): 27044-27053.
880 **Xu B, Cheval C, Laohavisit A, Hocking B, Chiasson D, Olsson TSG, Shirasu K, Faulkner**
881 **C, Gilliham M. 2017.** A calmodulin-like protein regulates plasmodesmal closure during
882 bacterial immune responses. *New Phytol* **215**(1): 77-84.
883 **Yeh YH, Chang YH, Huang PY, Huang JB, Zimmerli L. 2015.** Enhanced Arabidopsis
884 pattern-triggered immunity by overexpression of cysteine-rich receptor-like kinases. *Front*
885 *Plant Sci* **6**: 322.
886 **Yip Delormel T, Boudsocq M. 2019.** Properties and functions of calcium-dependent protein
887 kinases and their relatives in Arabidopsis thaliana. *New Phytol* **224**(2): 585-604.
888 **Yu TY, Sun MK, Liang LK. 2021.** Receptors in the Induction of the Plant Innate Immunity.
889 *Mol Plant Microbe Interact* **34**(6): 587-601.
890 **Yuan M, Cai B, Xin XF. 2023.** Plant immune receptor pathways as a united front against
891 pathogens. *PLoS Pathog* **19**(2): e1011106.
892 **Yuan M, Jiang Z, Bi G, Nomura K, Liu M, Wang Y, Cai B, Zhou JM, He SY, Xin XF.**
893 **2021a.** Pattern-recognition receptors are required for NLR-mediated plant immunity.
894 *Nature* **592**(7852): 105-109.
895 **Yuan M, Ngou BPM, Ding P, Xin XF. 2021b.** PTI-ETI crosstalk: an integrative view of plant
896 immunity. *Curr Opin Plant Biol* **62**: 102030.
897 **Zhang W, Fraiture M, Kolb D, Loffelhardt B, Desaki Y, Boutrot FF, Tor M, Zipfel C,**
898 **Gust AA, Brunner F. 2013.** Arabidopsis receptor-like protein30 and receptor-like kinase
899 suppressor of BIR1-1/EVERSHED mediate innate immunity to necrotrophic fungi. *Plant*
900 *Cell* **25**(10): 4227-4241.
901 **Zhou JM, Zhang Y. 2020.** Plant immunity: danger perception and signaling. *Cell* **181**(5): 978-
902 989.
903 **Zhou N, Tootle TL, Tsui F, Klessig DF, Glazebrook J. 1998.** PAD4 functions upstream from
904 salicylic acid to control defense responses in Arabidopsis. *Plant Cell* **10**(6): 1021-1030.

905

906 **Figure legends**

907 **Figure 1. Transcriptional reprogramming associated to BIR1 induction in Arabidopsis**

908 A) Morphology of representative BIR1 transgenic Arabidopsis plants (line 9, L9) under the
909 control of a DEX-inducible 35S promoter used for RNA-Seq experiments. Samples were
910 collected after 4 or 12 days of 30 µM DEX treatment. H_2O-treated plants were used as controls.
911 Relative BIR1 expression based on the number of Fragments Per Kilobase of transcript
912 sequence per Millions of base-pairs sequenced (FPKM) (top) and Western blot using anti-
913 mCherry antibody (bottom) in samples used for RNA-Seq. Significant differences between
914 DEX- and mock-treated samples were analyzed using two-way ANOVA followed by Sidak´s
915 multiple comparison test; ***, adjusted *p*-value < 0.001. B) Principal component analysis
916 (PCA) of RNA-Seq data. The PCA was performed using normalized RNA-Seq data of DEGs
917 between BIR1 L9 and wild-type (WT) plants after 4 and 12 days of DEX treatment (DeL9_vs
918 DeWT_). Each biological replicate is represented in the score plot. The variance explained by
919 each component (%) is given in parentheses. The sample (DeL9_12) with differential
920 expression within the DEX-treated L9 group is indicated with black arrows in A and B. C)
921 Number of up-or down-regulated transcripts, with a $|\log_2$ (Fold-Change)$| \geq 1$ and adjusted *p*-
922 value ≤ 0.01, in each pairwise comparison is indicated. D) Scatterplot of selected gene ontology
923 (GO) terms of DEGs. GO terms between WT and BIR1 L9 plants at 4 and 12 days after DEX-
924 treatment (DeL9_ vs DeWT_) are shown. Dot size represents the count of different genes and
925 the color indicates significance of the term enrichment. GO terms with adjusted *p*-value < 0.05
926 are significantly enriched. The kinase term (indicated by an arrow) was exclusively assigned to
927 BIR1 L9 plants. WT, wild-type Col-0; L9, BIR1 L9 transgenic plants; De, DEX-treated plants;
928 Mo, Mock-treated plants; _4, 4 days of treatment; _12, 12 days of treatment.

929

930 **Figure 2. Effect of BIR1 induction on immune responses triggered by flg22 and nlp20**
931 **treatments**

932 A) Over time production of reactive oxygen species (ROS) in wild-type (WT) and BIR1 L6 and
933 L9 transgenic plants after treatment of Arabidopsis leaf disks with 1 µM flg22 (left) or H_2O
934 (right) as elicitors. Bars represent means ± SD of relative fluorescence units. B) Ethylene
935 accumulation in BIR1 L6 and L9 transgenic plants after treatment with H_2O (mock), flg22 and
936 nlp20 at 1 µM or 100 nM concentration as indicated. Bars represent average values ± SD.
937 Within each elicitor/mock treatment, differences between DEX-treated (DEX+) and controls

938 (DEX-) were analyzed by two-way ANOVA followed by Sidak´s multiple comparison test. C)
939 RT-qPCR analysis of the PTI-marker genes FRKY and PR1 at 45 min after treatment with H_2O
940 (mock) or 1 µM flg22, and determined in DEX-treated (DEX+) versus non-treated (DEX-)
941 samples. D) Immunoprecipitation of mCherry-BIR1 fusion proteins, indicated with an
942 arrowhead, from samples of BIR1 L6 and L9 plants used in A and B (left), and RT-qPCR
943 analysis of BIR1 transcripts in DEX-treated (DEX+) samples of BIR1 L6 and L9 plants used
944 in C (right). In all cases, RT-qPCR values from biologically independent samples were
945 normalized to the *CBP20* internal control, and related to H_2O (mock)-treated plants, set to a
946 value of 1. Data are means ± SD analyzed by Kruskal-Wallis test; *, adjusted *p*-value <0.05.
947 Experiments were repeated three times with similar results.

948

949 **Figure 3. BIR1 induction inhibits flg22- and poly(I:C)-triggered callose accumulation at**
950 **PD**

951 A, B) Callose spots at PD were visualized upon aniline blue staining of epidermal cells in
952 response to bacterial flg22 (A) or poly(I:C) (B) in BIR1 L9 transgenic Arabidopsis plants.
953 Plants were previously treated with 30 µM DEX to elicit BIR1 expression. Mock-treated plants
954 were used as non BIR1-expressing controls (top panels). Photographs were taken 30 minutes
955 after treatment with H_2O (control) or 1 µM flg22 or 50 ng/µl of poly(I:C). BIR1-mCherry
956 fluorescence in DEX-treated BIR1 L9 plants was confirmed within the same images. Inlays
957 show enlargements of the areas within the dashed boxes. Scale bar, 10 µm. C) Relative PD
958 callose content in flg22/poly(I:C)-treated and H_2O (control)-treated leaves from BIR1 L9 plants
959 previously treated with or without DEX as indicated. Callose content at PD in DEX-treated
960 wild-type (WT) plants in response to poly (I:C) is shown. D) flg22/poly(I:C)-induced callose
961 content at PD in the *sobir1-12* and *bir1-1 sobir1-1* mutants. H_2O-treated controls and callose
962 deposition at PD from WT Col-0 leaves are shown as controls. In all cases, black dots represent
963 the mean values of callose intensities in individual PD (>100) measured in three leaf discs taken
964 from at least three independent biological replicates per each treatment. Significant differences
965 between samples were analyzed by Kruskal-Wallis test or by one-way ANOVA followed by
966 Tukey's multiple comparison test; ****, adjusted *p*-value <0.0001, ***, <0.001, **, <0.01.
967 Experiments were repeated twice with similar results.

968

969 **Figure 4. BIR1 overexpression leads to the transcriptional activation of PTI-associated**
970 **co-receptors and ETI regulators**

971 (A) Validation of the RNA-Seq results. Differential expression of selected BIR1-responsive
972 DEGs after 12 days of DEX treatment based on fold-change values (log_2 DeL9_12/DeWT_12
973 and log_2 DeL9_12/MoL9_12 as indicated) was confirmed by RT-qPCR. Values from
974 biologically independent samples were normalized to the *CBP20* internal control, and related
975 to untreated (DEX-) plants, set to a value of 1. Data are mean ± SD analyzed by Mann-Whitney
976 test; *, p <0.05. B) Relative expression of selected PTI/ETI-related genes based on the number
977 of Fragments Per Kilobase of transcript sequence per Millions of base-pairs sequenced (FPKM)
978 in each of the three independent samples per condition used for RNA-Seq. Actin expression is
979 shown as control. Note that the expression levels of each individual replicate within the DEX-
980 treated BIR1 L9_12 group mirror the abundance of BIR1 transcripts in each replicate.
981 Significant differences between mock-treated and DEX-treated samples were analyzed using
982 two-way ANOVA followed by Sidak´s multiple comparison test; ****, adjusted p-value <
983 0.0001, *** < 0.001, **< 0.01. WT, wild-type Col-0; L9, BIR1 L9 transgenics; _4d, 4 days of
984 treatment; _12d, 12 days of treatment. C) Western blot analysis of SOBIR1 and PR1 using
985 specific antibodies in two independent sets of BIR1 L9 samples. Plants were mock-treated (-)
986 or DEX-treated (+) for 12 days. The presence (+) or absence (-) of morphological phenotypes
987 (Ph) in each sample is indicated. Protein loading control by Ponceau S is shown.

988

989 **Figure 5. Phenotypes caused by BIR1 overexpression are partially rescued in *sobir1-12***
990 **mutants, but not in a *bak1-5* mutant**

991 A) Morphology of transgenic *sobir1-12* BIR1 L6 and *bak1*-5 BIR1 L10 mutant plants
992 expressing BIR1 under the control of a DEX-inducible 35S promoter. Transgenic BIR1 L9
993 plants in the wild-type (WT) Col-0 background are shown as a reference. Plants were grown
994 for three weeks on soil and treated with 30 µM DEX to induce BIR1 transcription or mock-
995 treated with H_2O. Non-transgenic WT Col-0 plants are shown as controls. Plants were
996 photographed after 12 days of the first DEX/ H_2O application. Images from independent
997 transgenic lines are shown in Fig. S7. RT-qPCR analysis of *BIR1* transcripts in BIR1 L9 plants
998 are shown. B) RT-qPCR analysis of *BIR1* and *EDS1* transcripts in *sobir1-12* BIR1 L6 and *bak1-*
999 5 BIR1 L10 plants. C) Western blot analysis of BIR1 and EDS1 proteins with specific
1000 antibodies in WT BIR1 L9 and two independent lines of *sobir1-12* BIR1 (L6, L8) and *bak1*-5

1001 BIR1 (L4, L10). Plants were mock-treated (-) or DEX-treated (+) for 12 days as indicated. The
1002 presence (+) or absence (-) of morphological phenotypes (Ph) in each sample is indicated.
1003 Protein loading control by Ponceau S is shown. D, E) RT-qPCR analysis of the PTI-marker
1004 genes RBOHD, FRKY or WKY29 in *sobir1-12* BIR1 L6 (D) and *bak1*-5 BIR1 L10 (E) plants.
1005 F, G) RT-qPCR analysis of representative marker genes of the salicylic acid (*PR1*), jasmonic
1006 acid (*PDF1.2*), ethylene (*PR4*) and camalexin (*PAD3, CYP79B2*) pathways in *sobir1-12* BIR1
1007 L6 (F) and *bak1*-5 BIR1 L10 (G) plants. In all cases, the same set of replicates from each
1008 genotype was used to measure all the genes shown in the graphs. Transcript accumulation was
1009 determined in mock-treated (DEX-) versus DEX-treated (DEX+) after 12 days of treatment.
1010 Values from biologically independent samples were normalized to the *CBP20* internal control,
1011 and related to mock-treated plants, set to a value of 1. Data are mean ± SD analyzed by Mann-
1012 Whitney test; *, p <0.05. Experiments were repeated at least twice with similar results.

1013

1014 **Figure 6. Phenotypes caused by BIR1 overexpression are partially rescued in *eds1-2***
1015 **mutants, but not in a *pad4-1* mutant**

1016 A) Morphology of transgenic *eds1-2* BIR1 L1b and *pad4-1* BIR1 L0 mutant plants expressing
1017 BIR1 under the control of a DEX-inducible 35S promoter. Plants were grown for three weeks
1018 on soil and treated with 30 µM DEX to induce BIR1 transcription or mock-treated with H_2O.
1019 Plants were photographed after 12 days of the first DEX/ H_2O application. Images from
1020 independent transgenic lines are shown in Fig. S7. RT-qPCR analysis of BIR1 transcript in
1021 *eds1-2* BIR1 L1b and *pad4-1* BIR1 L0 mutant lines are shown. B, C) RT-qPCR analysis of the
1022 PTI-marker genes *RBOHD* and *FRKY* in *eds1-2* BIR1 L1b (B) and *pad4-1* BIR1 L0 (C) plants.
1023 D, E) RT-qPCR analysis of representative marker genes of the salicylic acid (*PR1*), jasmonic
1024 acid (*PDF1.2*), ethylene (*PR4*) and camalexin (*PAD3, CYP79B2*) pathways in *eds1-2* BIR1 L1b
1025 (D) and *pad4-1* BIR1 L0 (E) plants. In all cases, the same set of replicates from each genotype
1026 was used to measure all the genes shown in the graphs. Transcript accumulation was determined
1027 in mock-treated (DEX-) versus DEX-treated (DEX+) after 12 days of treatment. Values from
1028 biologically independent samples were normalized to the *CBP20* internal control, and related
1029 to mock-treated plants, set to a value of 1. Data are mean ± SD analyzed by Mann-Whitney test;
1030 *, p <0.05. Experiments were repeated at least twice with similar results.

1031

1032 **Figure 7. Phenotypes caused by BIR1 overexpression are independent of salicylic acid**
1033 **(SA)-mediated signaling pathways**

1034 A) Morphology of transgenic *sid2-2* BIR1 (L5) and *eds5-3* BIR1 (L10) mutant plants
1035 expressing BIR1 under the control of a DEX-inducible 35S promoter. Plants were grown for
1036 three weeks on soil and treated with 30 µM DEX to induce BIR1 transcription or mock-treated
1037 with H_2O. Plants were photographed after 12 days of the first DEX/ H_2O application. Images
1038 from independent transgenic lines are shown in Fig. S7A,B. B, C) RT-qPCR analysis of BIR1
1039 and representative marker genes of the jasmonic acid (*PDF1.2*) and camalexin (*PAD3,*
1040 *CYP79B2*) pathways in *sid2-2* BIR1 (L5) (B) and *eds5-3* BIR1 (L10) (C) mutant lines. In all
1041 cases, the same set of replicates from each genotype was used to measure all the genes shown
1042 in the graphs. Transcript accumulation was determined in mock-treated (DEX-) versus DEX-
1043 treated (DEX+) after 12 days of treatment. Values from biologically independent samples were
1044 normalized to the *CBP20* internal control, and related to mock-treated plants, set to a value of
1045 1. Data are mean ± SD analyzed by Mann-Whitney test; *, $p < 0.05$. Experiments were repeated
1046 at least twice with similar results. D) Tentative working model for BIR1 homeostasis. SA-
1047 mediated transcription of BIR1 is regulated by RNA-directed DNA methylation (RdDM) and
1048 post-transcriptional RNA silencing (PTGS) (Guzman-Benito *et al.*, 2019). In these conditions,
1049 BIR1 induction interferes with PTI gene expression and PD callose deposition triggered by
1050 various elicitors (flg22, nlp20, dsRNA). Loss of BIR1 regulation leads to constitutive BIR1
1051 induction and ultimately BIR1 overexpression at levels that cause SA-independent up-
1052 regulation of immune and hormone genes. BIR1 overexpression is sensed by one or several
1053 TNLs, of which CSA1 is a plausible candidate, to promote PAD4-independent ETI-type cell
1054 death that requires EDS1 and SOBIR1.

1055

1056

1057 **Supporting information**

1058 **Figure S1. Transcriptomic profiling of BIR1 expressing transgenic lines**

1059 A) Principal component analysis (PCA) of RNA-Seq data. The PCA was performed using
1060 normalized RNA-Seq data of DEGs between DEX-treated and mock-treated transgenic BIR1
1061 L9 plants after 4 and 12 days of treatment (DeL9_vs MoL9_). Each biological replicate is
1062 represented in the score plot. The variance explained by each component (%) is given in
1063 parentheses. B) Number of up-or down-regulated transcripts, with a $|\log_2 (\text{Fold-Change})| \geq 1$
1064 and adjusted *p*-value ≤0.05, in each pairwise comparison as indicated. C) Volcano plots
1065 showing the distribution of DEGs (adjusted *p*-value ≤ 0.05). The x-axis shows the fold change
1066 in gene expression between samples, and y-axis shows the statistical significance of the
1067 differences. Significantly up- and down-regulated genes are highlighted in red and green,
1068 respectively. Genes that are not differentially regulated are in blue. C) Scatterplot of selected
1069 gene ontology (GO) terms of DEGs. GO terms between wild-type (WT) and BIR1 L9 plants at
1070 4 and 12 days after DEX-treatment (DeL9_ vs MoL9_) are shown. Dot size represents the count
1071 of different genes and the color indicates significance of the term enrichment. GO terms with
1072 adjusted *p*-value < 0.05 are significantly enriched. The kinase term (indicated by an arrow) was
1073 exclusively assigned to BIR1 L9 plants. WT, wild-type Col-0; L9, BIR1 L9 transgenic plants;
1074 De, DEX-treated plants; Mo, Mock-treated plants; _4, 4 days of treatment; _12, 12 days of
1075 treatment.

1076

1077 **Figure S2. Transcriptomic profiling of DEX-treated wild-type Col-0 plants**

1078 A) Morphology of representative wild-type (WT) Arabidopsis plants used for RNA-Seq
1079 experiments. Samples were collected after 4 or 12 days of 30 μM DEX treatment and subjected
1080 to RNA sequencing. H_2O-treated plants were used as controls. Note that application of DEX
1081 has a negative effect on plant growth as deduced by the significant reduction of rosette size
1082 after 12 days of DEX treatment relative to the non-treated controls. Box and whisker plot
1083 showing 5-95 percentile was analyzed by Mann-Whitney test; ****, *p* <0.0001. B) Volcano
1084 plots showing the distribution of DEGs (adjusted *p*-value ≤ 0.05). The x-axis shows the gene
1085 fold change, and y-axis plots the statistical significance (*p*-value) of the differences.
1086 Significantly up- and down-regulated genes are highlighted in red and green, respectively.
1087 Genes that are not differentially regulated are in blue. C) Principal component analysis (PCA)
1088 of RNA-Seq data. The PCA was performed using normalized RNA-Seq data of DEGs between

1089 DEX-treated and mock-treated WT plants after 4 and 12 days of treatment (DeWT_vs
1090 MoWT_). Each biological replicate is represented in the score plot. The variance explained by
1091 each component (%) is given in parentheses. D) Scatterplot of selected gene ontology (GO)
1092 terms of DEGs. GO terms between DEX-treated and mock-treated WT plants at 4 and 12 days
1093 of treatment (DeL9_ vs MoL9_) are shown. Dot size represents the count of different genes and
1094 the color indicates significance of the term enrichment. GO terms with adjusted *p*-value < 0.05
1095 are significantly enriched. WT, wild-type Col-0; De, DEX-treated plants; Mo, Mock-treated
1096 plants; _4, 4 days of treatment; _12, 12 days of treatment.

1097

1098 **Figure S3. Enrichment analysis of Kyoto Encyclopedia of Genes and Genomes (KEGG)**
1099 **pathways using RNA-Seq data**

1100 Scatterplot of selected Kyoto Encyclopedia of Genes and Genomes (KEGG) pathways. Dot size
1101 represents the count of different genes and the color indicates significance of the term
1102 enrichment. Terms with adjusted *p*-value < 0.05 are significantly enriched. WT, wild-type Col-
1103 0; De, DEX-treated plants; Mo, Mock-treated plants; _4, 4 days of treatment; _12, 12 days of
1104 treatment.

1105

1106 **Figure S4. Differential expression of RLP-coding genes in BIR1 overexpressing plants**

1107 A) Relative expression levels of selected RLP-coding genes based on the number of Fragments
1108 Per Kilobase of transcript sequence per Millions of base-pairs sequenced (FPKM) in each of
1109 the three independent samples per condition used for RNA-Seq. Significant differences
1110 between DEX- and mock-treated samples were analyzed using two-way ANOVA followed by
1111 Sidak´s multiple comparison test; ***, adjusted *p*-value < 0.001, **< 0.01. Note that the
1112 expression levels of each individual replicate within the DEX-treated BIR1 L9_12 group mirror
1113 the abundance of BIR1 transcripts in each replicate. B) Differential expression of selected
1114 BIR1-responsive RLP-coding genes based on $\log_2$ fold-change in the indicated pairwise
1115 comparisons. WT, wild-type Col-0; L9, BIR1 L9 transgenics; De, DEX-treated plants; Mo,
1116 mock-treated plants: _4d, 4 days of treatment; _12d, 12 days of treatment.

1117

1118 **Figure S5. Differential expression of cysteine-rich RLK (CRK)-coding genes in BIR1**
1119 **overexpressing plants**

1120 A) Relative expression levels of selected CRK-coding genes based on the number of Fragments
1121 Per Kilobase of transcript sequence per Millions of base-pairs sequenced (FPKM) in each of
1122 the three independent samples per condition used for RNA-Seq. Significant differences
1123 between DEX- and mock-treated samples were analyzed using two-way ANOVA followed by
1124 Sidak´s multiple comparison test; ***, adjusted *p*-value < 0.001, **< 0.01. Note that the
1125 expression levels of each individual replicate within the DEX-treated BIR1 L9_12 group mirror
1126 the abundance of BIR1 transcripts in each replicate. B) Differential expression of selected
1127 BIR1-responsive CRK-coding genes based on $\log_2$ fold-change in the indicated pairwise
1128 comparisons. WT, wild-type Col-0; L9, BIR1 L9 transgenics; De, DEX-treated plants; Mo,
1129 mock-treated plants: _4d, 4 days of treatment; _12d, 12 days of treatment.

1130

1131 **Figure S6. Differential expression of cell-surface pattern recognition receptors (PRR) and**
1132 **calcium-dependent protein kinases (CPK)-encoding genes in BIR1 overexpressing plants**

1133 A, B) Relative expression levels of selected PRR- and CPK-coding genes based on the number
1134 of Fragments Per Kilobase of transcript sequence per Millions of base-pairs sequenced (FPKM)
1135 in each of the three independent samples per condition used for RNA-Seq. Significant
1136 differences between DEX- and mock-treated samples were analyzed using two-way ANOVA
1137 followed by Sidak´s multiple comparison test; ***, adjusted *p*-value < 0.001, **< 0.01, *< 0.05.
1138 WT, wild-type Col-0; L9, BIR1 L9 transgenics; De, DEX-treated plants; Mo, mock-treated
1139 plants: _4d, 4 days of treatment; _12d, 12 days of treatment.

1140

1141 **Figure S7. Morphological and growth defects in BIR1 overexpressing plants of different**
1142 **PTI/ETI mutant genetic backgrounds**

1143 A) Morphology of transgenic *sobir1-12* BIR1 L8, *bak1-5* BIR1 L4, *eds1*-2 BIR1 L2, *pad4-1*
1144 BIR1 L12b and *eds5-3* BIR1 L12 mutant plants from independent lines expressing BIR1 under
1145 the control of a DEX-inducible 35S promoter. Plants were grown for three weeks on soil and
1146 treated with 30 µM DEX to activate BIR1 transcription or mock-treated with H_2O. Plants were
1147 photographed after 12 days of the first DEX/ H2O application. B) Morphology and BIR1
1148 expression levels of DEX- and mock-treated *sobir1-12* BIR1 (L6, L8) and *bak1-5* BIR1 (L4,
1149 L10) plants as observed in different biological replicates of the experiment. qRT-PCR analysis
1150 showed comparable BIR1 transcript levels in both genotypes. Each sample consisted of RNA
1151 pooled from six different plants. C) RT-qPCR analysis of the PTI-marker WRK29 gene in

1152 *sobir1-12* BIR1 L6 and *pad4*-1 BIR1 L10 mutant backgrounds. In all cases, transcript
1153 accumulation was determined in DEX-treated (DEX+) versus mock-treated (DEX-) after 12
1154 days of treatment. Values from biologically independent samples were normalized to the
1155 CBP20 internal control, and related to mock-treated plants, set to a value of 1. Data are mean ±
1156 SD analyzed by Mann-Whitney test; *, $p < 0.05$. D) Rosette size (diameter) in wild-type (WT)
1157 and BIR1 overexpressing ETI/PTI mutants after 12 days of DEX treatment relative to the non-
1158 treated controls. Box and whisker plots showing 5-95 percentile were analyzed by Mann-
1159 Whitney test; ****, $p < 0.0001$. Note that rosette size is largely influenced by the effect of DEX
1160 on plant development as shown for WT Col-0 plant in this study.

1161

1162 **Table S1. List of primers**

1163 **Table S2. List of expressed genes**

1164 Values represent the total read counts/ Fragments Per Kilobase of transcript sequence per
1165 Millions of base-pairs sequenced (FRKM) values of each biological replicate (a,b,c) per
1166 condition and their corresponding row mean values. De (DEX-treated plants), Mo (Mock-
1167 treated plants), WT (wild-type plants), L9 (BIR1 L9 transgenic plants), _4 (4 days of treatment),
1168 _12 (12 days of treatment).

1169

1170 **Table S3. List of differentially expressed genes (DEG. padjust value < 0.05)**

1171 Values represent the mean Fragments Per Kilobase of transcript sequence per Millions of base-
1172 pairs sequenced (FPKM) values from three biological replicates per condition. De (DEX-
1173 treated plants), Mo (Mock-treated plants), WT (wild-type plants), L9 (BIR1 L9 transgenic
1174 plants), _4 (4 days of treatment), _12 (12 days of treatment).

1175

1176 **Table S4. List of differentially expressed genes (DEG. |Log2fold change > 1| padjust value**
1177 **< 0.01)**

1178 Values represent the mean Fragments Per Kilobase of transcript sequence per Millions of base-
1179 pairs sequenced (FPKM) values from three biological replicates per condition. De (DEX-
1180 treated plants), Mo (Mock-treated plants), WT (wild-type plants), L9 (BIR1 L9 transgenic
1181 plants), _4 (4 days of treatment), _12 (12 days of treatment).

1182

1183 **Table S5. Enrichment analysis of Gene Ontology (GO) terms**

1184 CC (cellular component), BP (biological process) and MF (molecular function). Gene Ratio is
1185 the ratio of DEGs to all genes for this GO term. Bg Ratio is the ratio of all genes concerning
1186 this GO term to all genes in background GO database. Count is the number of differentially
1187 expressed genes concerning this GO term. Adjusted p-value < 0.05 means significant
1188 enrichment. De (DEX-treated plants), Mo (Mock-treated plants), WT (wild-type plants), L9
1189 (BIR1 L9 transgenic plants), _4 (4 days of treatment), _12 (12 days of treatment).

1190

1191 **Table S6. Kyoto Encyclopedia of Genes and Genomes (KEGG) pathway enrichment**
1192 **analysis**

1193 Gene Ratio is the ratio of DEGs to all genes for this pathway. Bg Ratio is the ratio of all genes
1194 concerning this KEGG term to all genes in background KEGG database. Count is the number
1195 of differentially expressed genes concerning this term. Adjusted p-value < 0.05 means
1196 significant enrichment. De (DEX-treated plants), Mo (Mock-treated plants), WT (wild-type
1197 plants), L9 (BIR1 L9 transgenic plants), _4 (4 days of treatment), _12 (12 days of treatment).

1198

1199 **Table S7. List of differentially expressed genes (DEG. padjust value < 0.05) within**
1200 **functional categories**

1201 Values represent the mean Fragments Per Kilobase of transcript sequence per Millions of base-
1202 pairs sequenced (FPKM) values from three biological replicates per condition. De (DEX-
1203 treated plants), Mo (Mock-treated plants), WT (wild-type plants), L9 (BIR1 L9 transgenic
1204 plants), _4 (4 days of treatment), _12 (12 days of treatment).

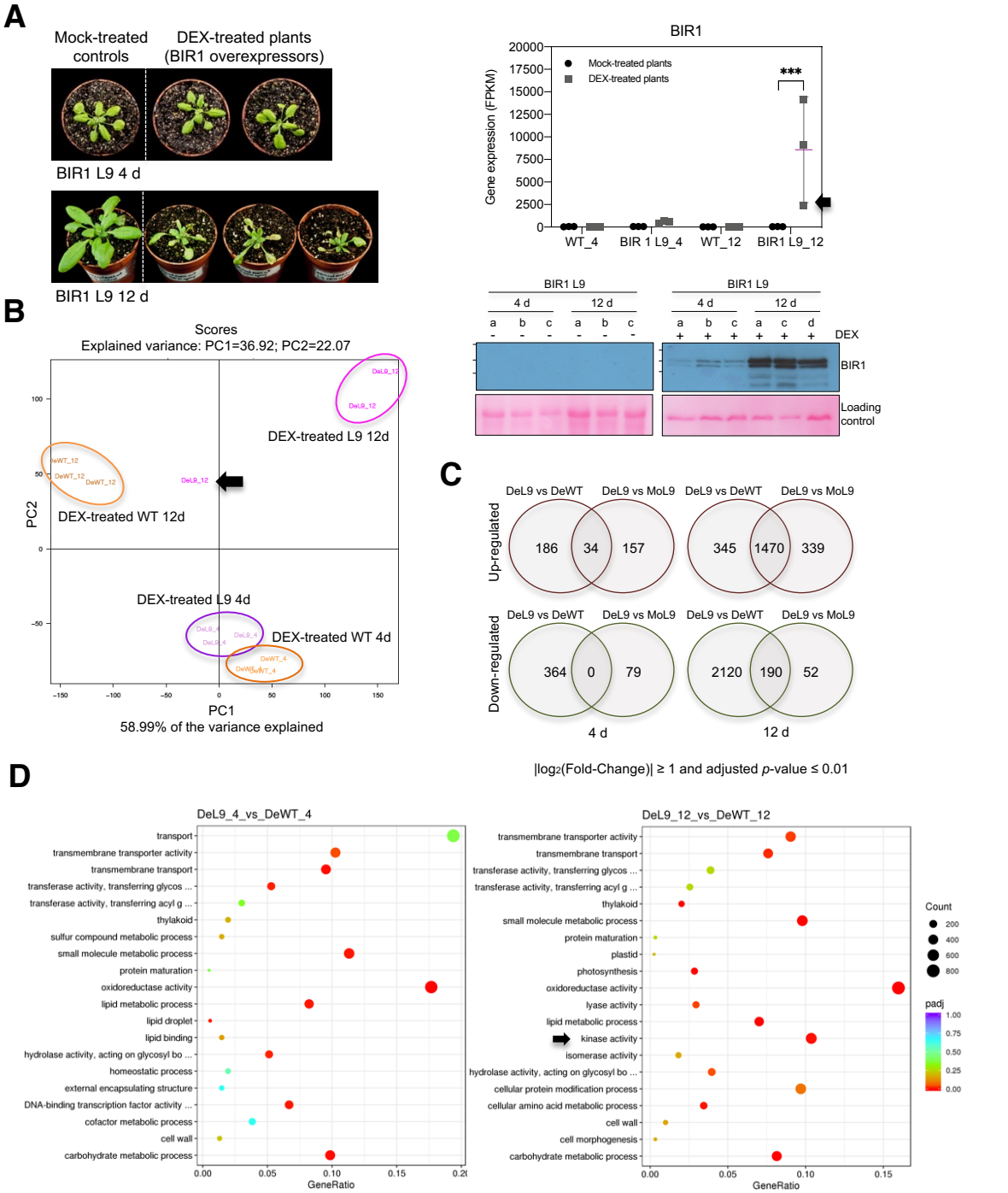

Figure 1. Transcriptional reprogramming associated to BIR1 induction in Arabidopsis.

A) Morphology of representative BIR1 transgenic Arabidopsis plants (line 9, L9) under the control of a DEX-inducible 35S promoter used for RNA-Seq experiments. Samples were collected after 4 or 12 days of 30 µM DEX treatment. H_2O-treated plants were used as controls. Relative BIR1 expression based on the number of Fragments Per Kilobase of transcript sequence per Millions of base-pairs sequenced (FPKM) (top) and Western blot using anti-mCherry antibody (bottom) in samples used for RNA-Seq. Significant differences between DEX- and mock-treated samples were analyzed using two-way ANOVA followed by Sidak´s multiple comparison test; ***, adjusted *p*-value < 0.001. B) Principal component analysis (PCA) of RNA-Seq data. The PCA was performed using normalized RNA-Seq data of DEGs between BIR1 L9 and wild-type (WT) plants after 4 and 12 days of DEX treatment (DeL9_vs DeWT_). Each biological replicate is represented in the score plot. The variance explained by each component (%) is given in parentheses. The sample (DeL9_12) with differential expression within the DEX-treated L9 group is indicated with black arrows in A and B. C) Number of up-or down-regulated transcripts, with a $|\log_2(\text{Fold-Change})| \geq 1$ and adjusted *p*-value ≤0.01, in each pairwise comparison is indicated. D) Scatterplot of selected gene ontology (GO) terms of DEGs. GO terms between WT and BIR1 L9 plants at 4 and 12 days after DEX-treatment (DeL9_ vs DeWT_) are shown. Dot size represents the count of different genes and the color indicates significance of the term enrichment. GO terms with adjusted *p*-value < 0.05 are significantly enriched. The kinase term (indicated by an arrow) was exclusively assigned to BIR1 L9 plants. WT, wild-type Col-0; L9, BIR1 L9 transgenic plants; De, DEX-treated plants; Mo, Mock-treated plants; _4, 4 days of treatment; _12, 12 days of treatment.

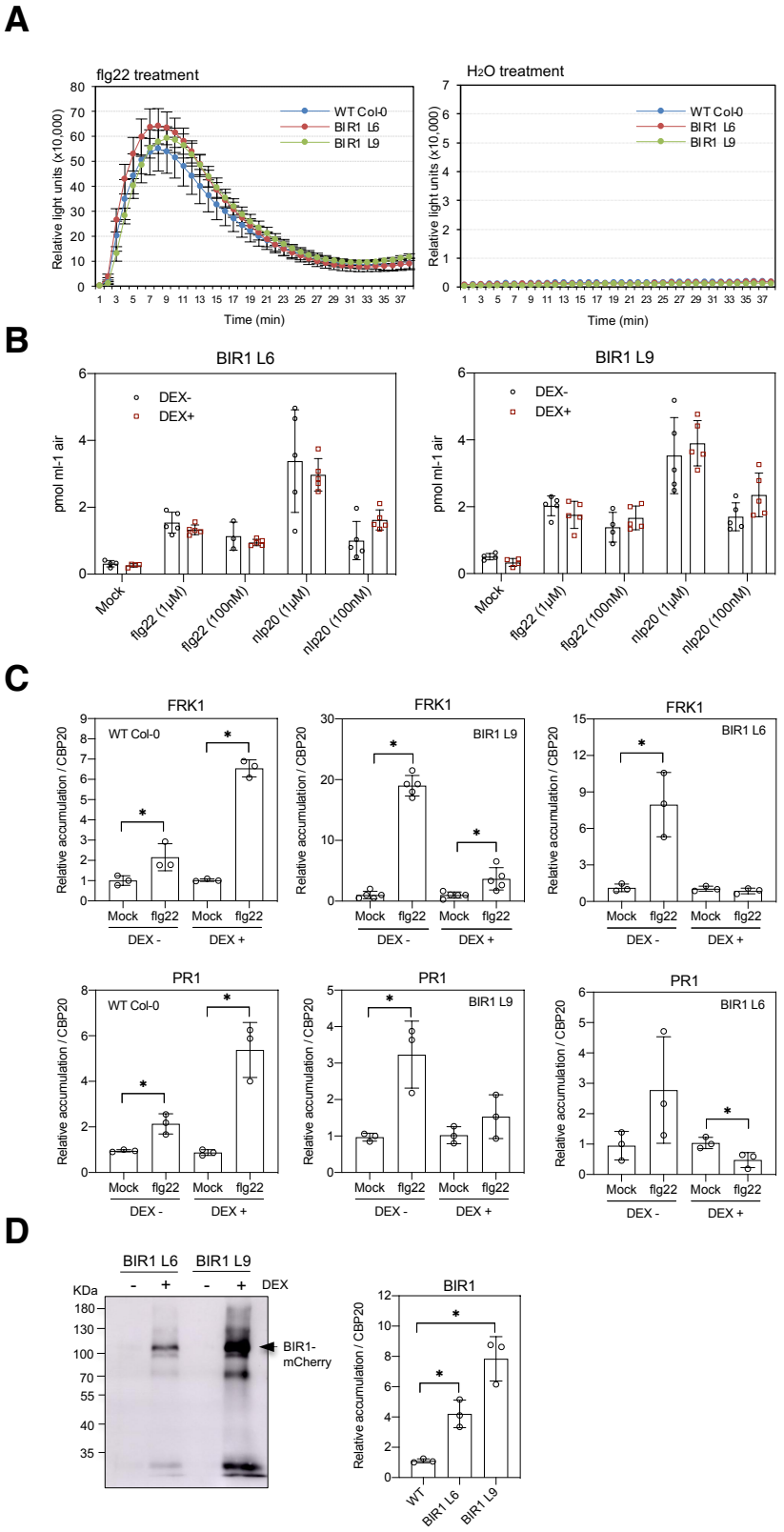

Figure 2. Effect of BIR1 induction on immune responses triggered by flg22 and nlp20 treatments

A) Over time production of reactive oxygen species (ROS) in wild-type (WT) and BIR1 L6 and L9 transgenic plants after treatment of Arabidopsis leaf disks with 1 µM flg22 (left) or H_2O (right) as elicitors. Bars represent means ± SD of relative fluorescence units. B) Ethylene accumulation in BIR1 L6 and L9 transgenic plants after treatment with H_2O (mock), flg22 and nlp20 at 1 µM or 100 nM concentration as indicated. Bars represent average values ± SD. Within each elicitor/mock treatment, differences between DEX-treated (DEX+) and controls (DEX-) were analyzed by two-way ANOVA followed by Sidak´s multiple comparison test. C) RT-qPCR analysis of the PTI-marker genes FRKY and PR1 at 45 min after treatment with H_2O (mock) or 1 µM flg22, and determined in DEX-treated (DEX+) versus non-treated (DEX-) samples. D) Immunoprecipitation of mCherry-BIR1 fusion proteins, indicated with an arrowhead, from samples of BIR1 L6 and L9 plants used in A and B (left), and RT-qPCR analysis of BIR1 transcripts in DEX-treated (DEX+) samples of BIR1 L6 and L9 plants used in C (right). In all cases, RT-qPCR values from biologically independent samples were normalized to the *CBP20* internal control, and related to H_2O (mock)-treated plants, set at 1. Data are means ± SD analyzed by Kruskal-Wallis test; *, adjusted *p*-value <0.05. Experiments were repeated three times with similar results.

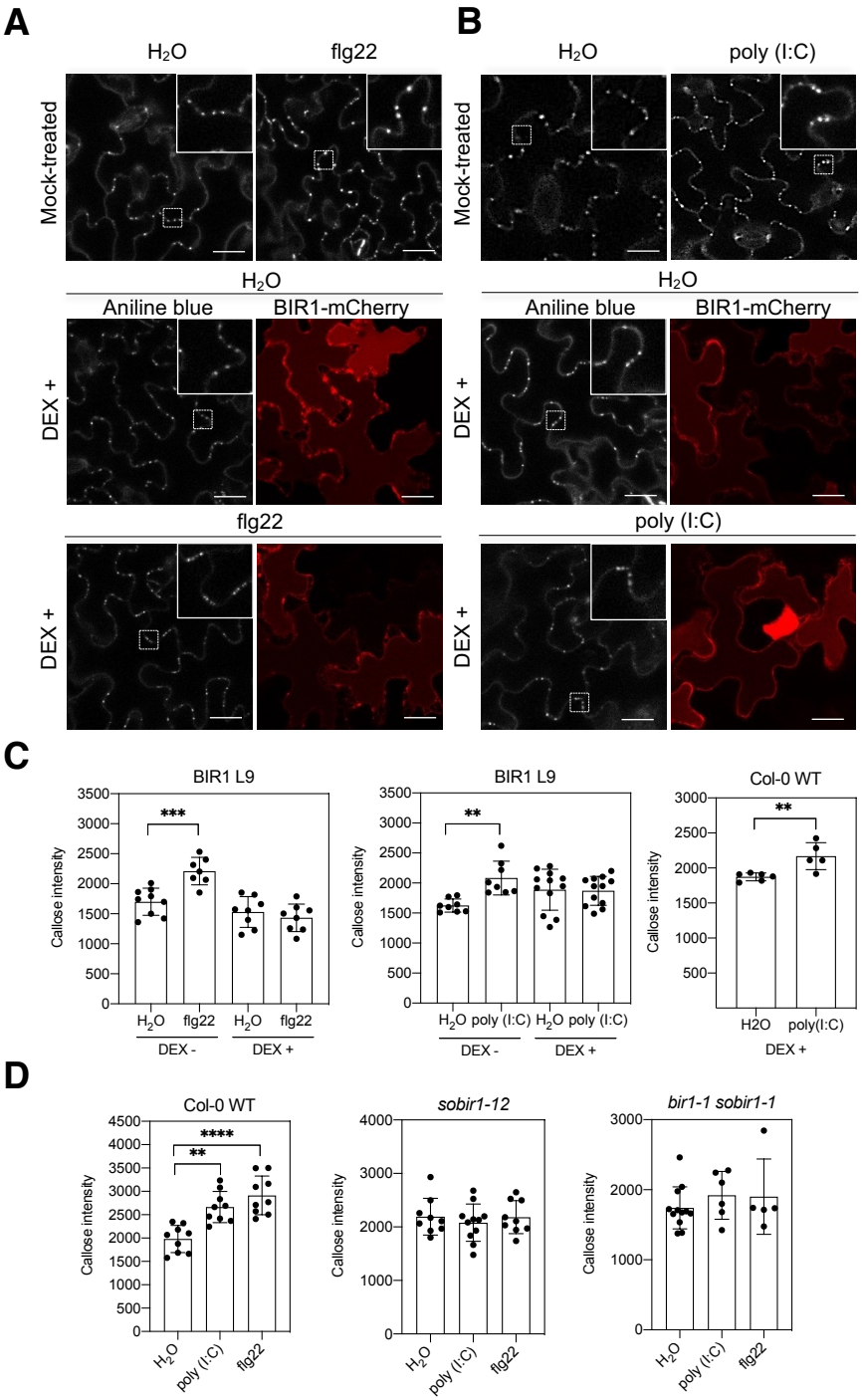

Figure 3. BIR1 induction inhibits flg22- and poly(I:C)-triggered callose accumulation at PD

A, B) Callose spots at PD were visualized upon aniline blue staining of epidermal cells in response to bacterial flg22 (A) or poly(I:C) (B) in BIR1 L9 transgenic Arabidopsis plants. Plants were previously treated with 30 µM DEX to elicit BIR1 expression. Mock-treated plants were used as non BIR1-expressing controls (top panels). Photographs were taken 30 minutes after treatment with H_2O (control) or 1 µM flg22 or 50 ng/µl of poly(I:C). BIR1-mCherry fluorescence in DEX-treated BIR1 L9 plants was confirmed within the same images. Inlays show enlargements of the areas within the dashed boxes. Scale bar, 10 µm. C) Relative PD callose content in flg22/poly(I:C)-treated and H_2O (control)-treated leaves from BIR1 L9 plants previously treated with or without DEX as indicated. Callose content at PD in DEX-treated wild-type (WT) plants in response to poly (I:C) is shown. D) flg22/poly(I:C)-induced callose content at PD in the *sobir1-12* and *bir1-1 sobir1-1* mutants. H_2O-treated controls and callose deposition at PD from WT Col-0 leaves are shown as controls. In all cases, black dots represent the mean values of callose intensities in individual PD (>100) measured in three leaf discs taken from at least three independent biological replicates per each treatment. Significant differences between samples were analyzed by Kruskal-Wallis test or by one-way ANOVA followed by Tukey's multiple comparison test; ****, adjusted *p*-value <0.0001, ***, <0.001, **, <0.01. Experiments were repeated twice with similar results.

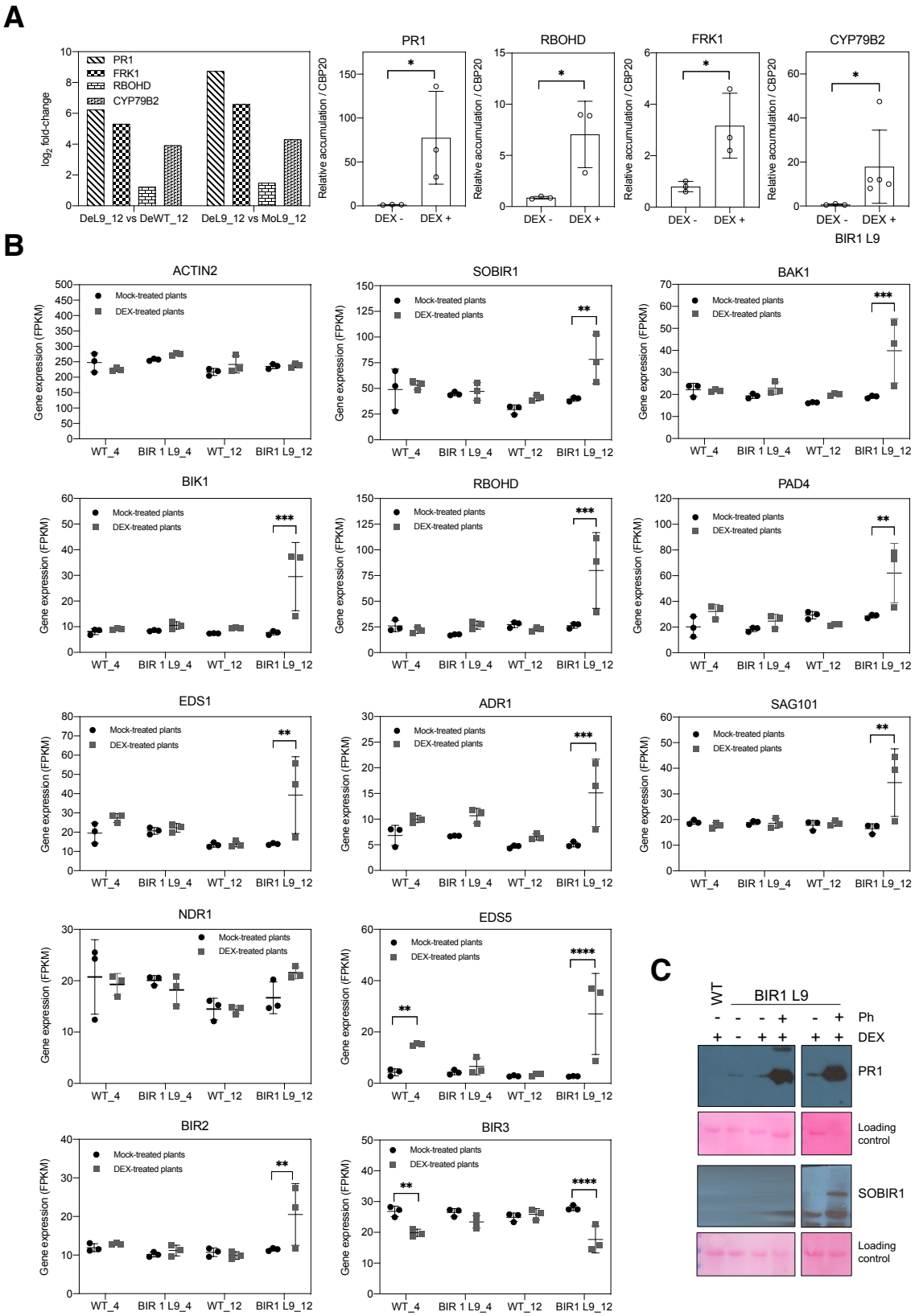

Figure 4. BIR1 overexpression leads to the transcriptional activation of PTI-associated co-receptors and ETI regulators

(A) Validation of the RNA-Seq results. Differential expression of selected BIR1-responsive DEGs after 12 days of DEX treatment based on fold-change values (log_2 DeL9_12/DeWT_12 and log_2 DeL9_12/MoL9_12 as indicated) was confirmed by RT-qPCR. Values from biologically independent samples were normalized to the *CBP20* internal control, and related to untreated (DEX-) plants, set at 1. Data are mean ± SD analyzed by Mann-Whitney test; *, p <0.05. B) Relative expression of selected PTI/ETI-related genes based on the number of Fragments Per Kilobase of transcript sequence per Millions of base-pairs sequenced (FPKM) in each of the three independent samples per condition used for RNA-Seq. Actin expression is shown as control. Note that the expression levels of each individual replicate within the DEX-treated BIR1 L9_12 group mirror the abundance of BIR1 transcripts in each replicate. Significant differences between mock-treated and DEX-treated samples were analyzed using two-way ANOVA followed by Sidak´s multiple comparison test; ****, adjusted p-value < 0.0001, *** < 0.001, **< 0.01. WT, wild-type Col-0; L9, BIR1 L9 transgenics; _4d, 4 days of treatment; _12d, 12 days of treatment. C) Western blot analysis of SOBIR1 and PR1 using specific antibodies in two independent sets of BIR1 L9 samples. Plants were mock-treated (-) or DEX-treated (+) for 12 days. The presence (+) or absence (-) of morphological phenotypes (Ph) in each sample is indicated. Protein loading control by Ponceau S is shown.

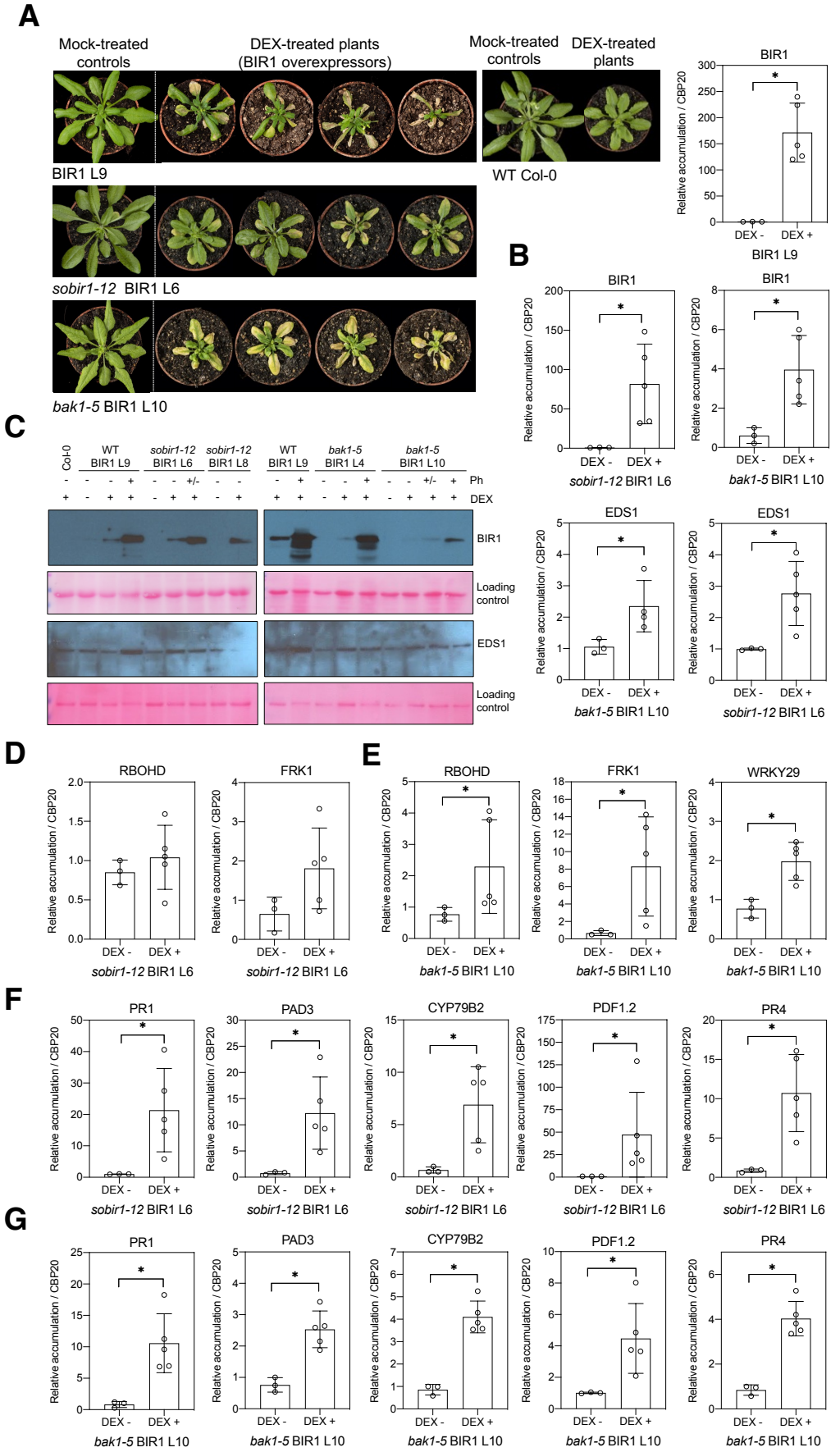

Figure 5. Phenotypes caused by BIR1 overexpression are partially rescued in *sobir1-12* mutants, but not in a *bak1-5* mutant.

A) Morphology of transgenic *sobir1-12* BIR1 L6 and *bak1*-5 BIR1 L10 mutant plants expressing BIR1 under the control of a DEX-inducible 35S promoter. Transgenic BIR1 L9 plants in the wild-type (WT) Col-0 background are shown as a reference. Plants were grown for three weeks on soil and treated with 30 µM DEX to induce BIR1 transcription or mock-treated with H_2O. Non-transgenic WT Col-0 plants are shown as controls. Plants were photographed after 12 days of the first DEX/ H_2O application. Images from independent transgenic lines are shown in Fig. S7. RT-qPCR analysis of *BIR1* transcripts in BIR1 L9 plants are shown. B) RT-qPCR analysis of *BIR1* and *EDS1* transcripts in *sobir1-12* BIR1 L6 and *bak1*-5 BIR1 L10 plants. C) Western blot analysis of BIR1 and EDS1 proteins with specific antibodies in WT BIR1 L9 and two independent lines of *sobir1-12* BIR1 (L6, L8) and *bak1*-5 BIR1 (L4, L10). Plants were mock-treated (-) or DEX-treated (+) for 12 days as indicated. The presence (+) or absence (-) of morphological phenotypes (Ph) in each sample is indicated. Protein loading control by Ponceau S is shown. D, E) RT-qPCR analysis of the PTI-marker genes RBOHD, FRKY or WKY29 in *sobir1-12* BIR1 L6 (D) and *bak1*-5 BIR1 L10 (E) plants. F, G) RT-qPCR analysis of representative marker genes of the salicylic acid (*PR1*), jasmonic acid (*PDF1.2*), ethylene (*PR4*) and camalexin (*PAD3, CYP79B2*) pathways in *sobir1-12* BIR1 L6 (F) and *bak1*-5 BIR1 L10 (G) plants. In all cases, the same set of replicates from each genotype was used to measure all the genes shown in the graphs. Transcript accumulation was determined in mock-treated (DEX-) versus DEX-treated (DEX+) after 12 days of treatment. Values from biologically independent samples were normalized to the *CBP20* internal control, and related to mock-treated plants, set at 1. Data are mean ± SD analyzed by Mann-Whitney test; *, $p < 0.05$. Experiments were repeated at least twice with similar results.

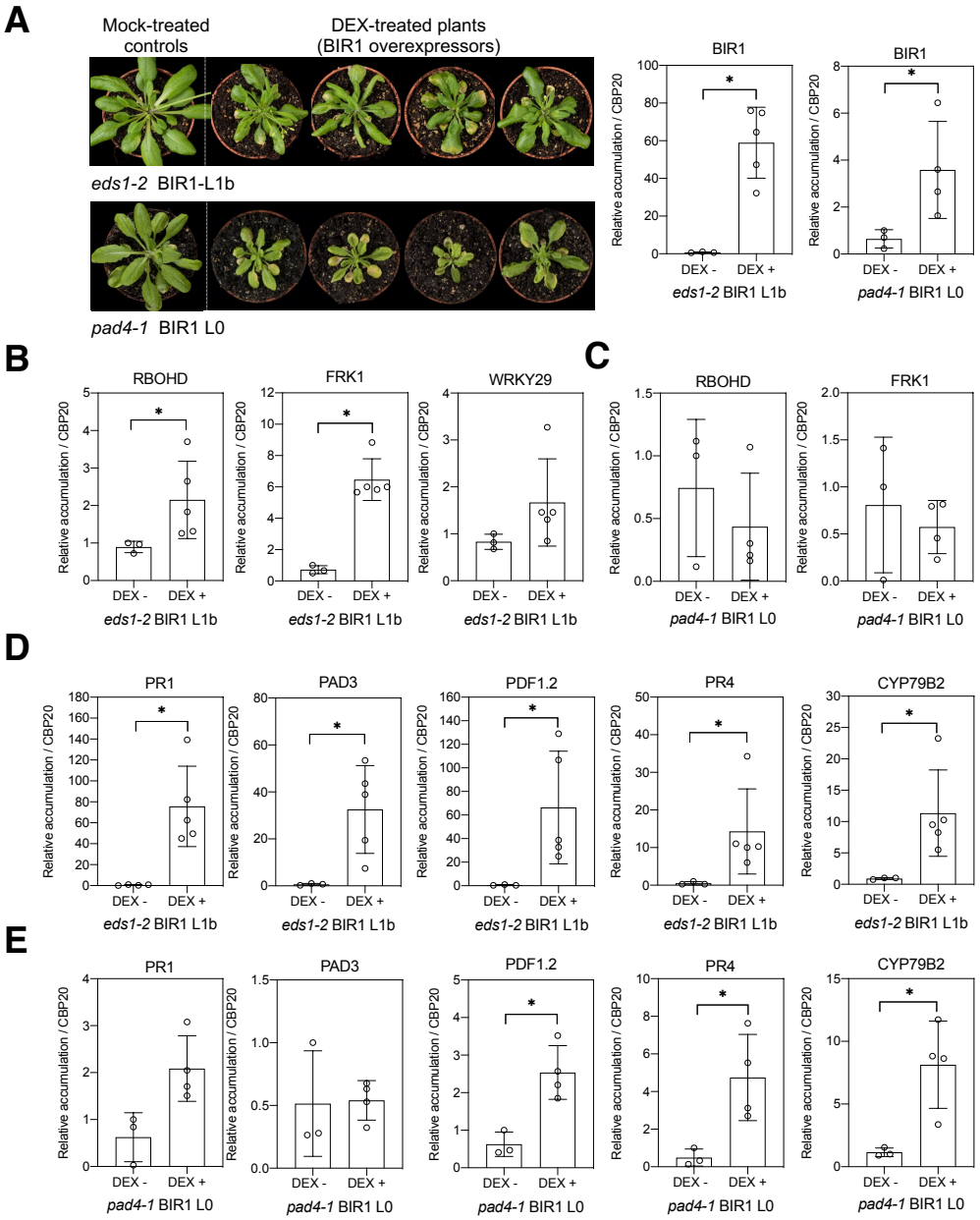

Figure 6. Phenotypes caused by BIR1 overexpression are partially rescued in *eds1-2* mutants, but not in a *pad4-1* mutant.

A) Morphology of transgenic *eds1-2* BIR1 L1b and *pad4-1* BIR1 L0 mutant plants expressing BIR1 under the control of a DEX-inducible 35S promoter. Plants were grown for three weeks on soil and treated with 30 µM DEX to induce BIR1 transcription or mock-treated with H_2O. Plants were photographed after 12 days of the first DEX/ H_2O application. Images from independent transgenic lines are shown in Fig. S7. RT-qPCR analysis of BIR1 transcript in *eds1-2* BIR1 L1b and *pad4-1* BIR1 L0 mutant lines are shown. B, C) RT-qPCR analysis of the PTI-marker genes *RBOHD* and *FRKY* in *eds1-2* BIR1 L1b (B) and *pad4-1* BIR1 L0 (C) plants. D, E) RT-qPCR analysis of representative marker genes of the salicylic acid (*PR1*), jasmonic acid (*PDF1.2*), ethylene (*PR4*) and camalexin (*PAD3, CYP79B2*) pathways in *eds1-2* BIR1 L1b (D) and *pad4-1* BIR1 L0 (E) plants. In all cases, the same set of replicates from each genotype was used to measure all the genes shown in the graphs. Transcript accumulation was determined in mock-treated (DEX-) versus DEX-treated (DEX+) after 12 days of treatment. Values from biologically independent samples were normalized to the *CBP20* internal control, and related to mock-treated plants, set at 1. Data are mean ± SD analyzed by Mann-Whitney test; *, $p < 0.05$. Experiments were repeated at least twice with similar results.

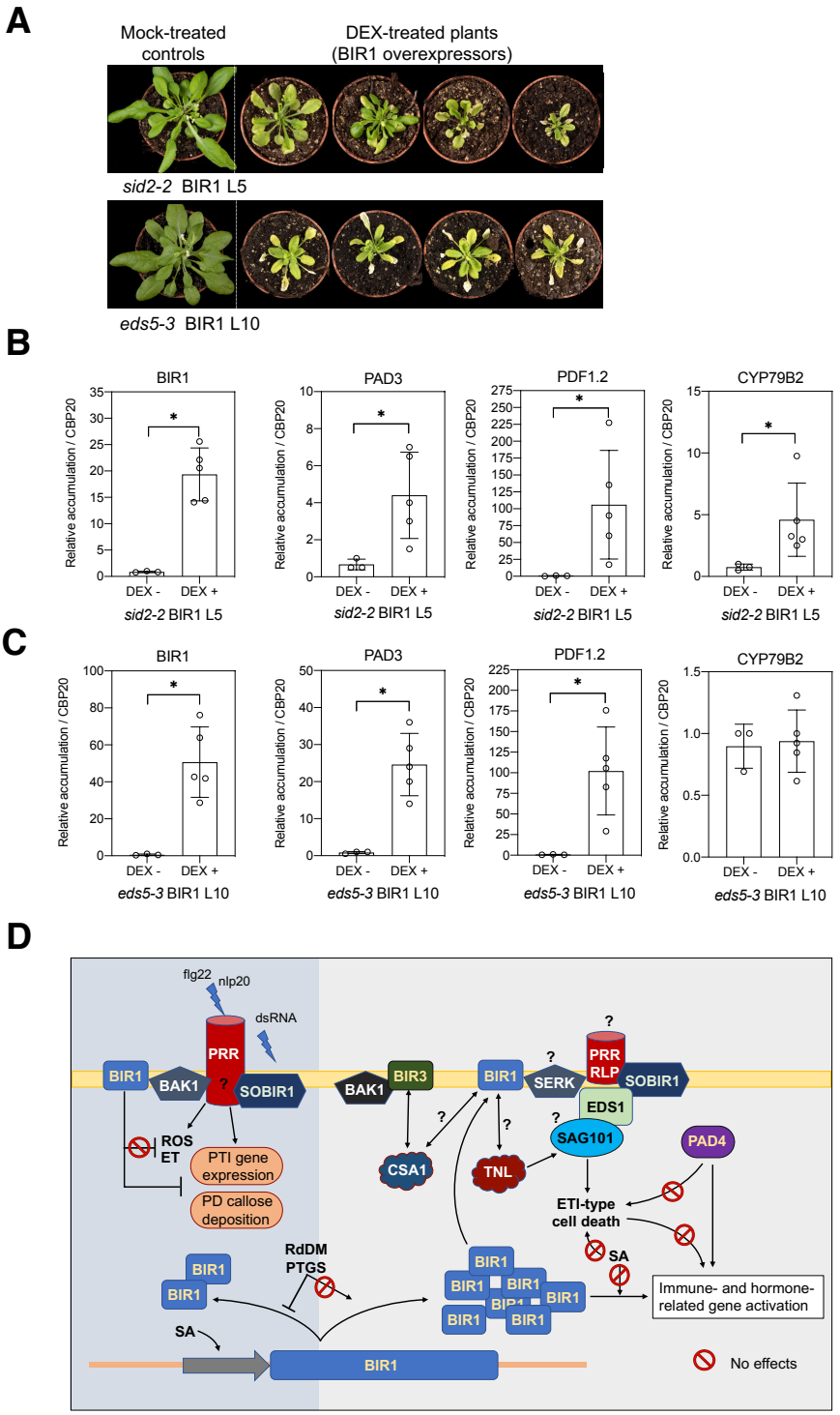

Figure 7. Phenotypes caused by BIR1 overexpression are independent of salicylic acid (SA)-mediated signaling pathways

A) Morphology of transgenic *sid2-2* BIR1 (L5) and *eds5-3* BIR1 (L10) mutant plants expressing BIR1 under the control of a DEX-inducible 35S promoter. Plants were grown for three weeks on soil and treated with 30 µM DEX to induce BIR1 transcription or mock-treated with H_2O. Plants were photographed after 12 days of the first DEX/ H_2O application. Images from independent transgenic lines are shown in Fig. S7. B, C) RT-qPCR analysis of BIR1 and representative marker genes of the jasmonic acid (*PDF1.2*) and camalexin (*PAD3, CYP79B2*) pathways in *sid2-2* BIR1 (L5) (B) and *eds5-3* BIR1 (L10) (C) mutant lines. In all cases, the same set of replicates from each genotype was used to measure all the genes shown in the graphs. Transcript accumulation was determined in mock-treated (DEX-) versus DEX-treated (DEX+) after 12 days of treatment. Values from biologically independent samples were normalized to the *CBP20* internal control, and related to mock-treated plants, set at 1. Data are mean ± SD analyzed by Mann-Whitney test; *, $p < 0.05$. Experiments were repeated at least twice with similar results. D) Tentative working model for BIR1 homeostasis. SA-mediated transcription of BIR1 is regulated by RNA-directed DNA methylation (RdDM) and post-transcriptional RNA silencing (PTGS) (Guzman-Benito *et al.*, 2019). In these conditions, BIR1 induction interferes with PTI gene expression and PD callose deposition triggered by various elicitors (flg22, nlp20, dsRNA). Loss of BIR1 regulation leads to constitutive BIR1 induction and ultimately BIR1 overexpression at levels that cause SA-independent up-regulation of immune and hormone genes. BIR1 overexpression is sensed by one or several TNLs, of which CSA1 is a plausible candidate, to promote PAD4-independent ETI-type cell death that requires EDS1 and SOBIR1.

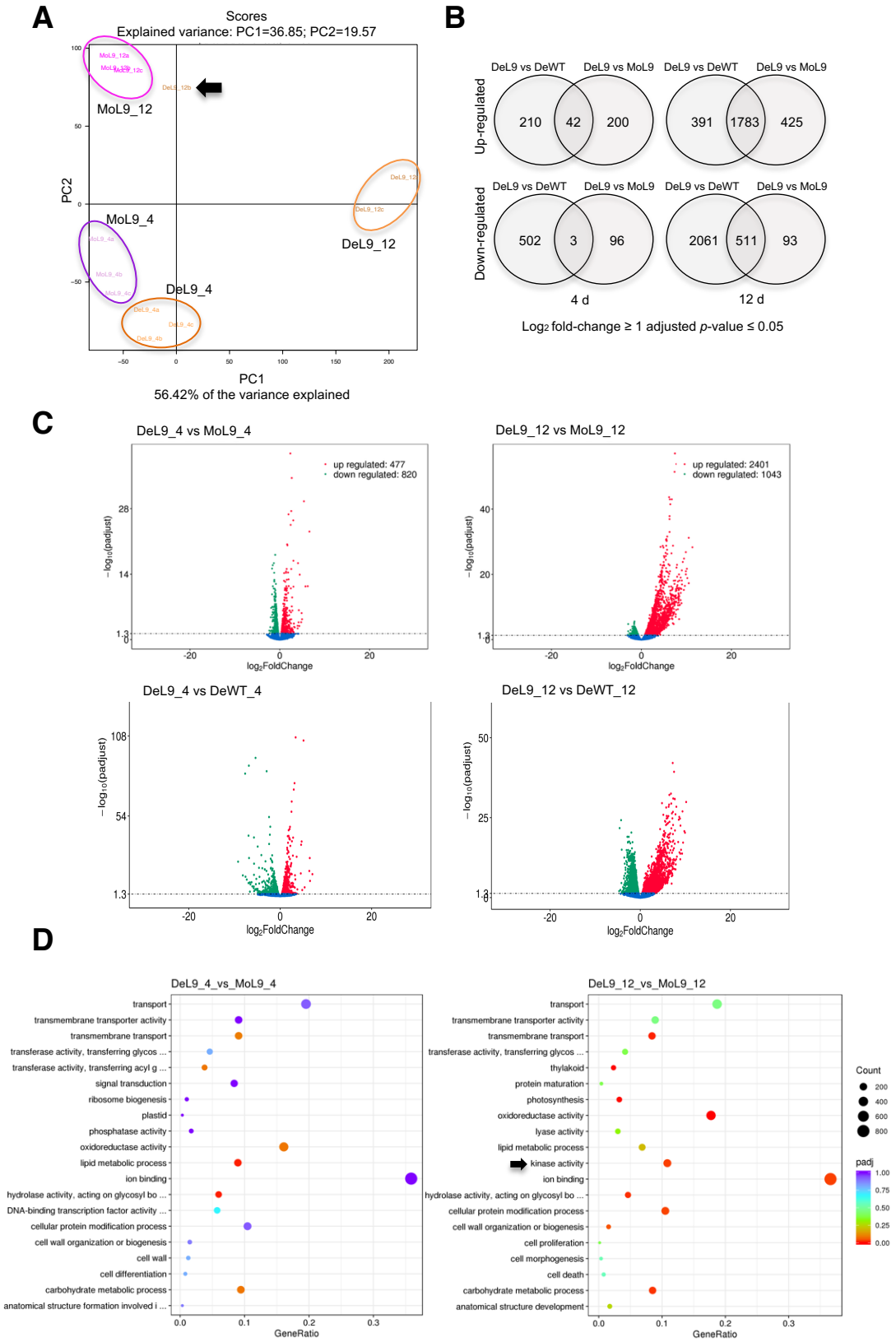

Figure S1. Transcriptomic profiling of BIR1 expressing transgenic lines.

A) Principal component analysis (PCA) of RNA-Seq data. The PCA was performed using normalized RNA-Seq data of DEGs between DEX-treated and mock-treated transgenic BIR1 L9 plants after 4 and 12 days of treatment (DeL9_vs MoL9_). Each biological replicate is represented in the score plot. The variance explained by each component (%) is given in parentheses. B) Number of up-or down-regulated transcripts, with a $|\log_2(\text{Fold-Change})| \geq 1$ and adjusted *p*-value ≤0.05, in each pairwise comparison as indicated. C) Volcano plots showing the distribution of DEGs (adjusted *p*-value ≤ 0.05). The x-axis shows the fold change in gene expression between samples, and y-axis shows the statistical significance of the differences. Significantly up- and down-regulated genes are highlighted in red and green, respectively. Genes that are not differentially regulated are in blue. C) Scatterplot of selected gene ontology (GO) terms of DEGs. GO terms between wild-type (WT) and BIR1 L9 plants at 4 and 12 days after DEX-treatment (DeL9_ vs MoL9_) are shown. Dot size represents the count of different genes and the color indicates significance of the term enrichment. GO terms with adjusted *p*-value < 0.05 are significantly enriched. The kinase term (indicated by an arrow) was exclusively assigned to BIR1 L9 plants. WT, wild-type Col-0; L9, BIR1 L9 transgenic plants; De, DEX-treated plants; Mo, Mock-treated plants; _4, 4 days of treatment; _12, 12 days of treatment.

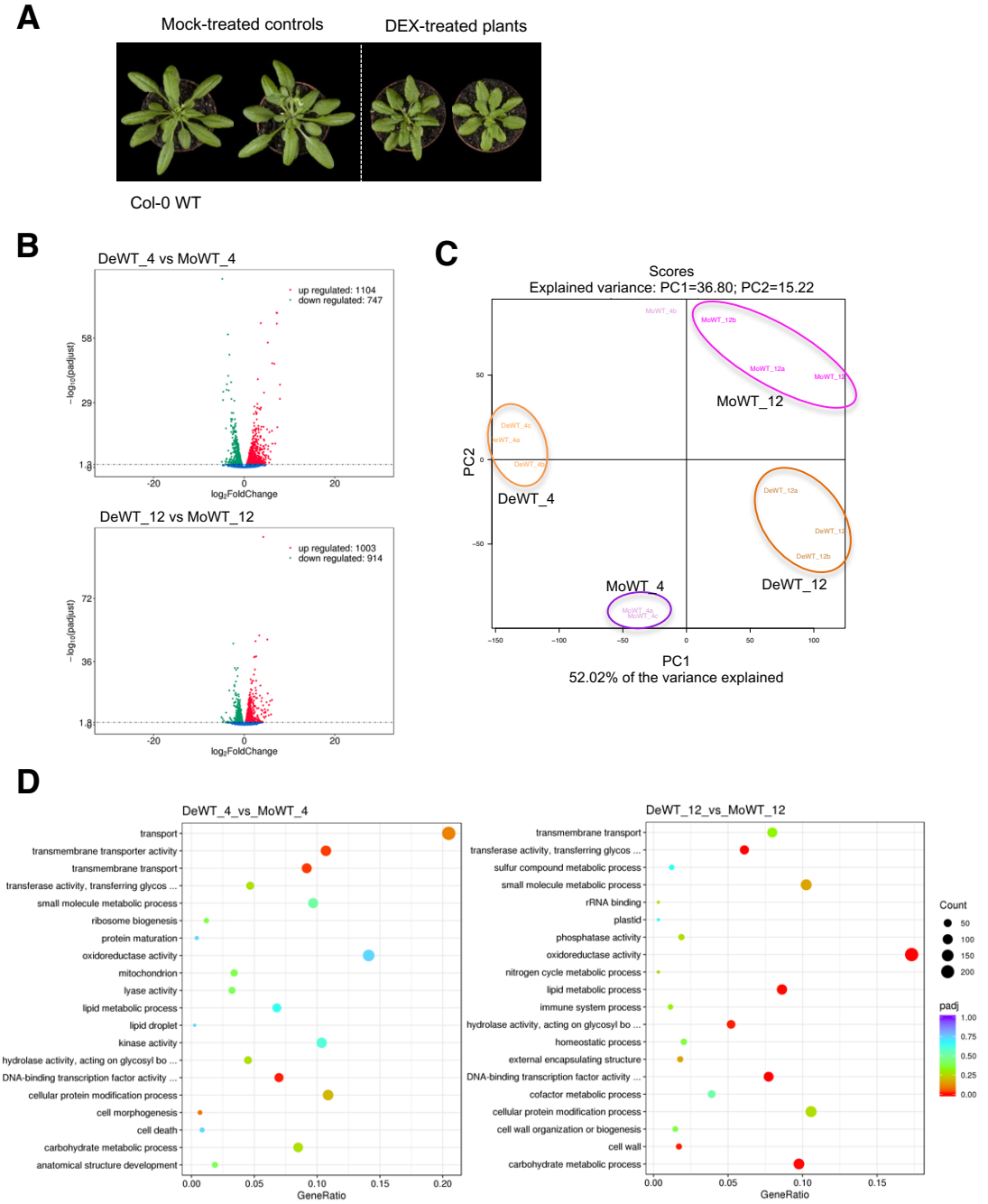

Figure S2. Transcriptomic profiling of DEX-treated wild-type Col-0 plants

A) Morphology of representative wild-type (WT) Arabidopsis plants used for RNA-Seq experiments. Samples were collected after 4 or 12 days of 30 µM DEX treatment and subjected to RNA sequencing. H_2O-treated plants were used as controls. Note that application of DEX has a negative effect on plant growth as deduced by the significant reduction of rosette size after 12 days of DEX treatment relative to the non-treated controls. Box and whisker plot showing 5-95 percentile was analyzed by Mann-Whitney test; ****, p <0.0001. B) Volcano plots showing the distribution of DEGs (adjusted p-value ≤ 0.05). The x-axis shows the gene fold change, and y-axis plots the statistical significance (p-value) of the differences. Significantly up- and down-regulated genes are highlighted in red and green, respectively. Genes that are not differentially regulated are in blue. C) Principal component analysis (PCA) of RNA-Seq data. The PCA was performed using normalized RNA-Seq data of DEGs between DEX-treated and mock-treated WT plants after 4 and 12 days of treatment (DeWT_vs MoWT_). Each biological replicate is represented in the score plot. The variance explained by each component (%) is given in parentheses. D) Scatterplot of selected gene ontology (GO) terms of DEGs. GO terms between DEX-treated and mock-treated WT plants at 4 and 12 days of treatment (DeL9_ vs MoL9_) are shown. Dot size represents the count of different genes and the color indicates significance of the term enrichment. GO terms with adjusted p-value < 0.05 are significantly enriched. WT, wild-type Col-0; De, DEX-treated plants; Mo, Mock-treated plants; _4, 4 days of treatment; _12, 12 days of treatment.

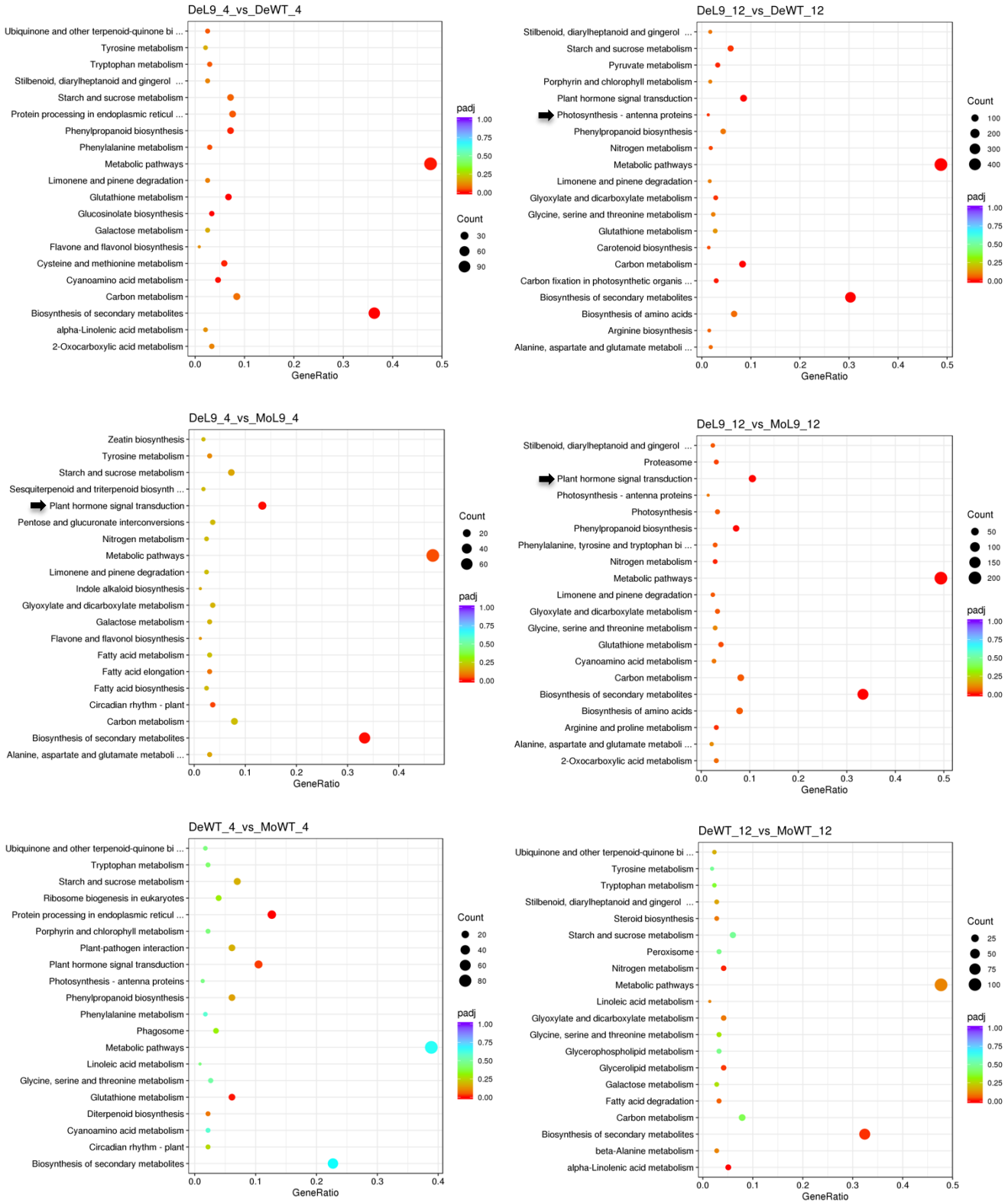

Figure S3. Enrichment analysis of Kyoto Encyclopedia of Genes and Genomes (KEGG) pathways using RNA-Seq data

Scatterplot of selected Kyoto Encyclopedia of Genes and Genomes (KEGG) pathways. Dot size represents the count of different genes and the color indicates significance of the term enrichment. Terms with adjusted *p*-value < 0.05 are significantly enriched. WT, wild-type Col-0; De, DEX-treated plants; Mo, Mock-treated plants; _4, 4 days of treatment; _12, 12 days of treatment.

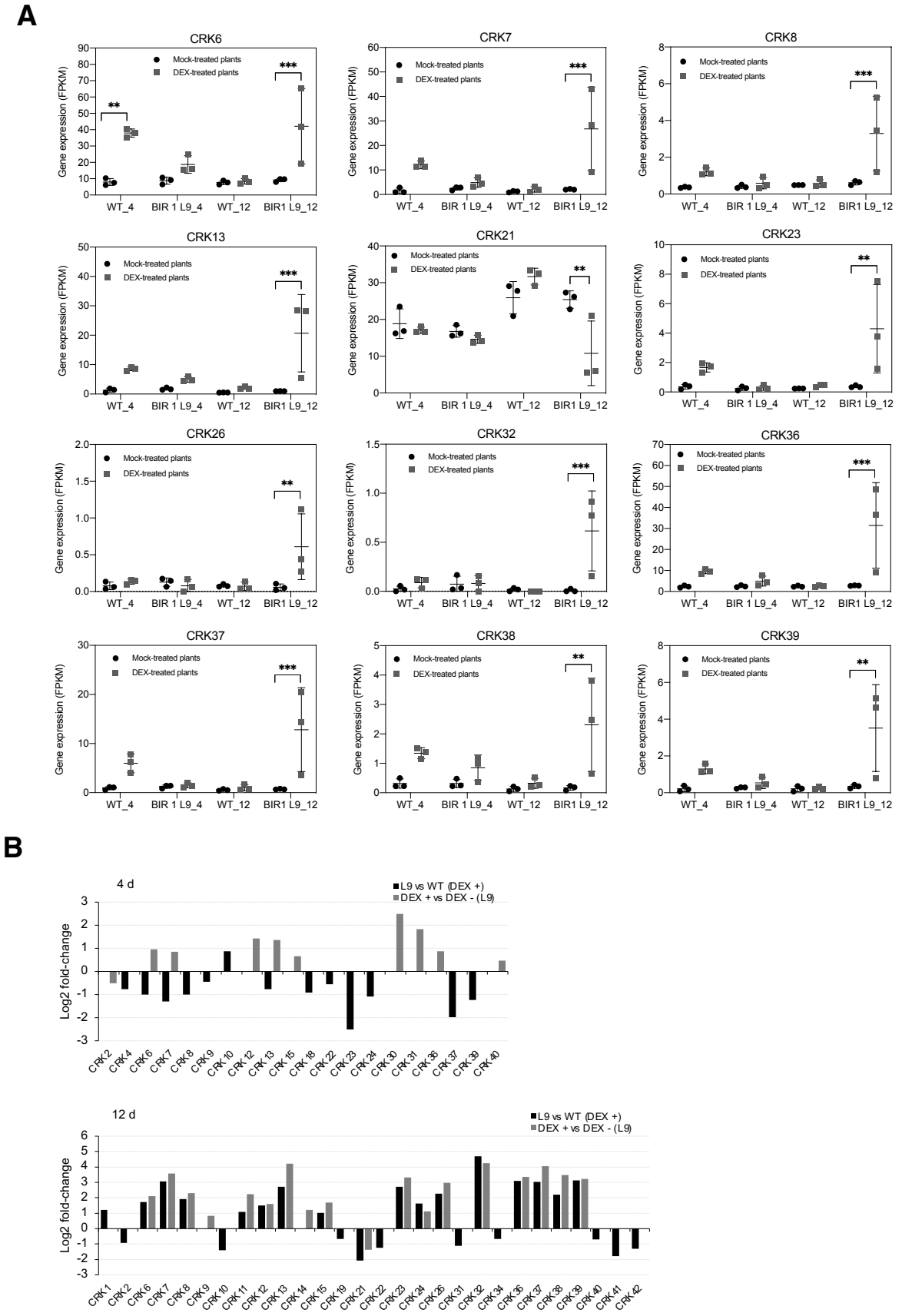

Figure S4. Differential expression of RLP-coding genes in BIR1 overexpressing plants

A) Relative expression levels of selected RLP-coding genes based on the number of Fragments Per Kilobase of transcript sequence per Millions of base-pairs sequenced (FPKM) in each of the three independent samples per condition used for RNA-Seq. Significant differences between DEX- and mock-treated samples were analyzed using two-way ANOVA followed by Sidak´s multiple comparison test; ***, adjusted *p*-value < 0.001, **< 0.01. Note that the expression levels of each individual replicate within the DEX-treated BIR1 L9_12 group mirror the abundance of BIR1 transcripts in each replicate. B) Differential expression of selected BIR1-responsive RLP-coding genes based on $\log_2$ fold-change in the indicated pairwise comparisons. WT, wild-type Col-0; L9, BIR1 L9 transgenics; De, DEX-treated plants; Mo, mock-treated plants: _4d, 4 days of treatment; _12d, 12 days of treatment

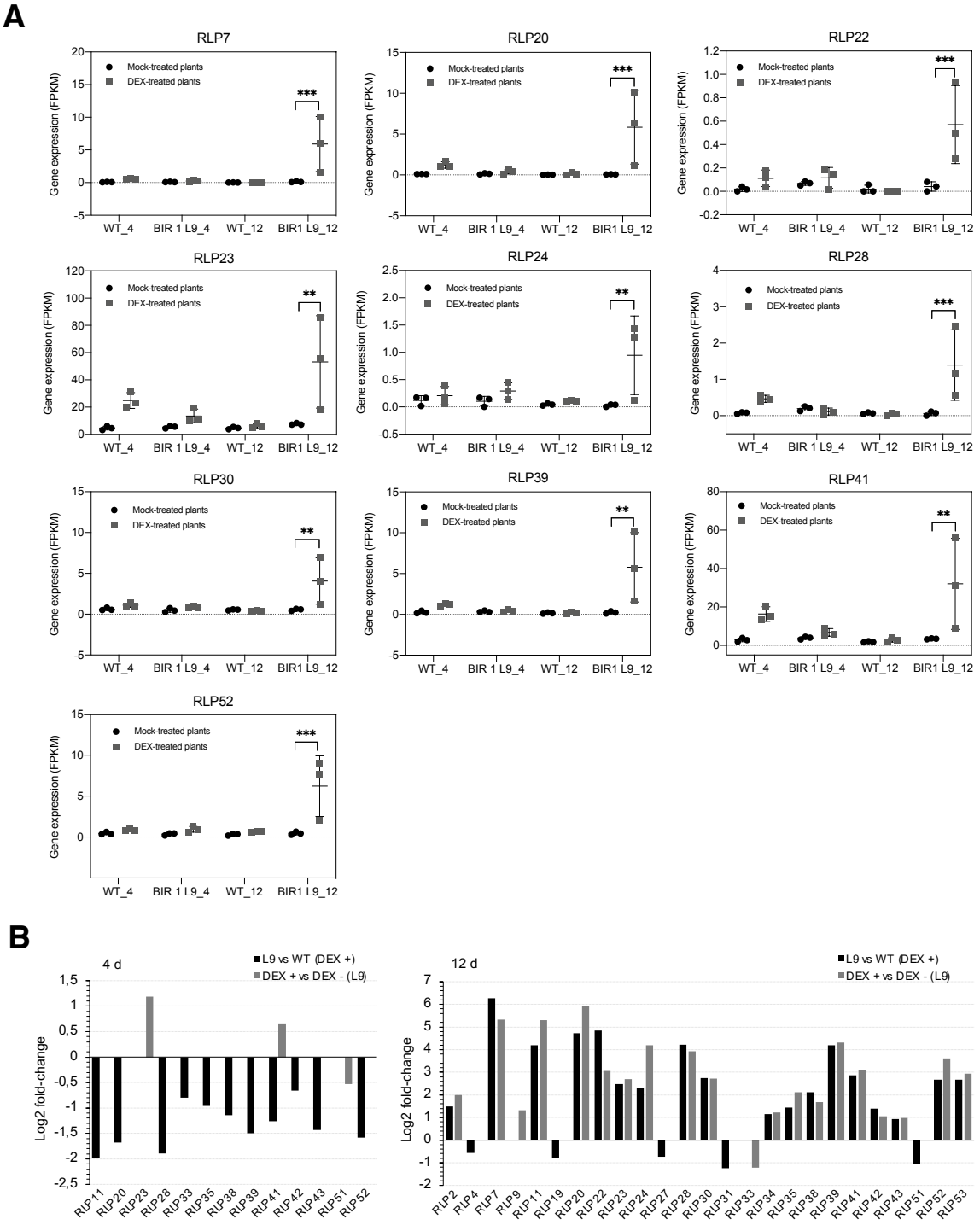

Figure S5. Differential expression of cysteine-rich RLK (CRK)-coding genes in BIR1 overexpressing plants

A) Relative expression levels of selected CRK-coding genes based on the number of Fragments Per Kilobase of transcript sequence per Millions of base-pairs sequenced (FPKM) in each of the three independent samples per condition used for RNA-Seq. Significant differences between DEX- and mock-treated samples were analyzed using two-way ANOVA followed by Sidak´s multiple comparison test; ***, adjusted *p*-value < 0.001, **< 0.01. Note that the expression levels of each individual replicate within the DEX-treated BIR1 L9_12 group mirror the abundance of BIR1 transcripts in each replicate. B) Differential expression of selected BIR1-responsive CRK-coding genes based on $\log_2$ fold-change in the indicated pairwise comparisons. WT, wild-type Col-0; L9, BIR1 L9 transgenics; De, DEX-treated plants; Mo, mock-treated plants: _4d, 4 days of treatment; _12d, 12 days of treatment

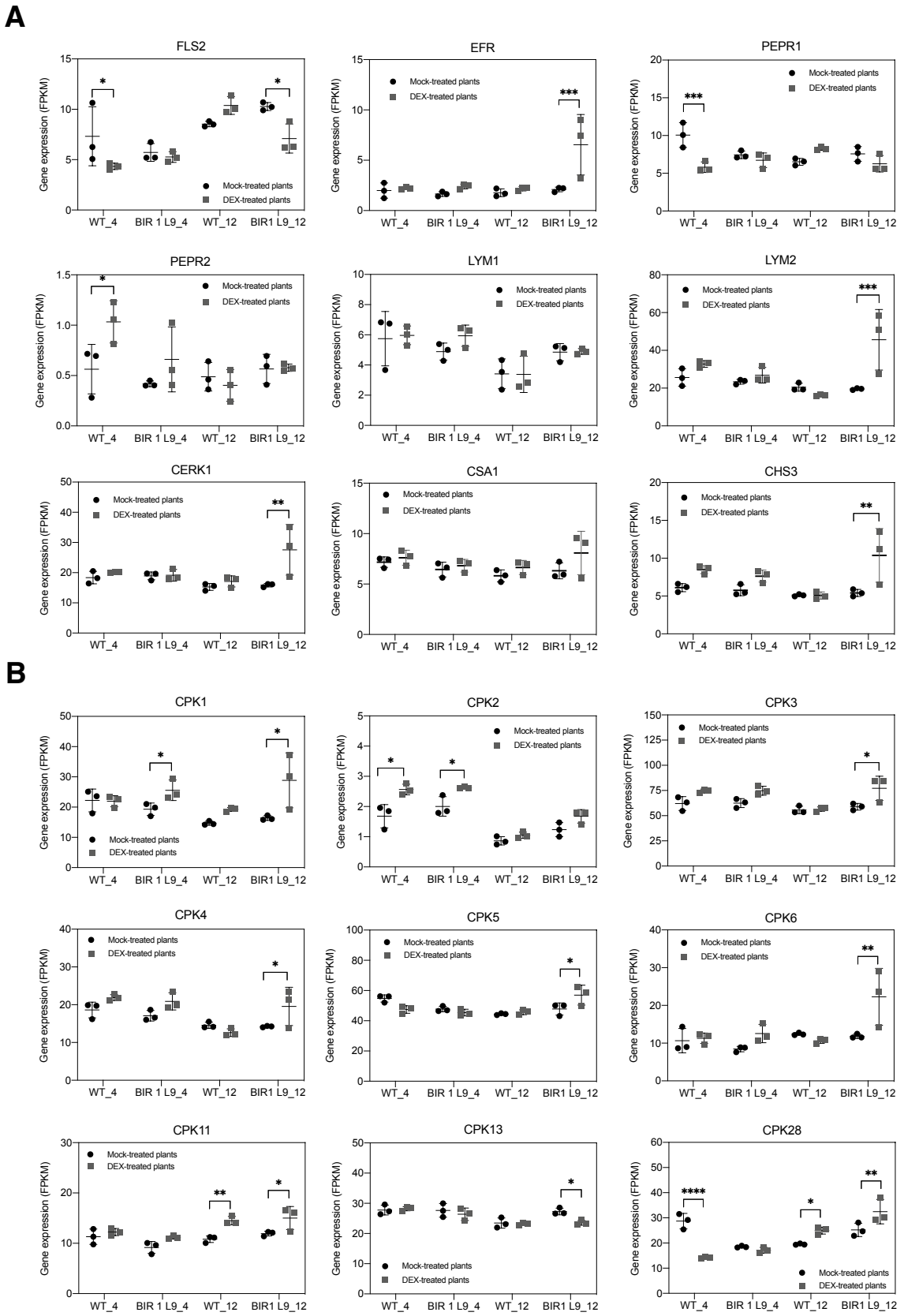

Figure S6. Differential expression of cell-surface pattern recognition receptors (PRR) and calcium-dependent protein kinases (CPK)-encoding genes in BIR1 overexpressing plants

A, B) Relative expression levels of selected PRR- and CPK-coding genes based on the number of Fragments Per Kilobase of transcript sequence per Millions of base-pairs sequenced (FPKM) in each of the three independent samples per condition used for RNA-Seq. Significant differences between DEX- and mock-treated samples were analyzed using two-way ANOVA followed by Sidak´s multiple comparison test; ***, adjusted *p*-value < 0.001, **< 0.01, *< 0.05. WT, wild-type Col-0; L9, BIR1 L9 transgenics; De, DEX-treated plants; Mo, mock-treated plants: _4d, 4 days of treatment; _12d, 12 days of treatment.

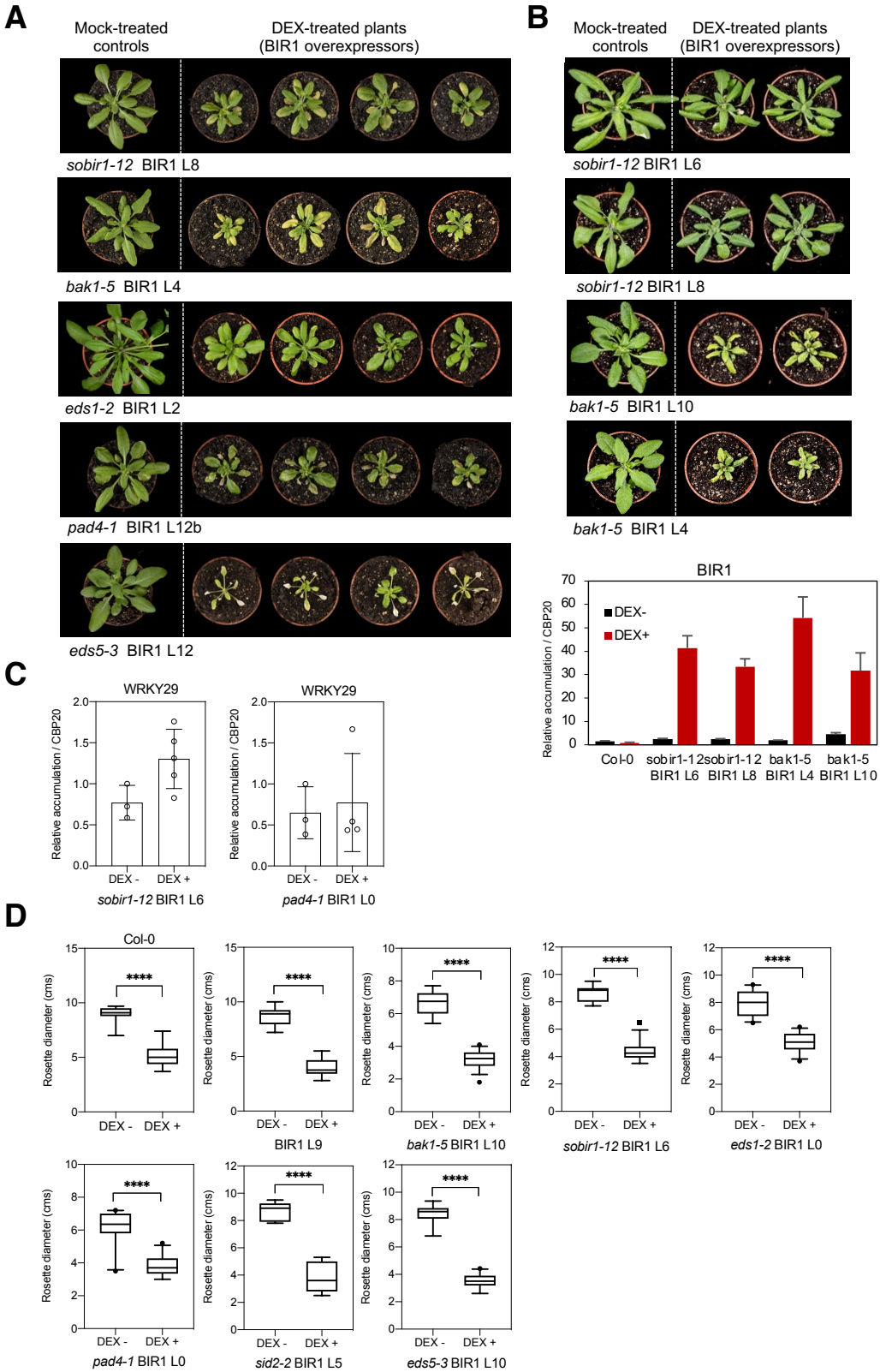

Figure S7. Morphological and growth defects in BIR1 overexpressing plants of different PTI/ETI mutant genetic backgrounds.

A) Morphology of transgenic Arabidopsis lines overexpressing BIR1 under the control of a DEX-inducible 35S promoter in the transfer DNA (T-DNA) insertional *bak1-5* (L4), *sobir1-12* (L8), *eds1-2* (L2), *pad4-1* (L12b) and *eds5-3* (L12) mutants. Plants were grown for three weeks on soil and treated with 30 µM DEX to activate BIR1 transcription or mock-treated with H_2O. Plants were photographed after 12 days of the first DEX/ H_2O application. B) Relative transcript accumulation of the PTI-marker *WRK29* gene in *bak1-5* BIR1 (L10) and *pad4-1* BIR1 (L10) mutant backgrounds. Relative transcript accumulation was determined in DEX-treated (DEX+) versus mock-treated (DEX-) after 12 days of treatment. RT-qPCR values from biologically independent samples were normalized to the *CBP20* internal control, and related to mock-treated plants, set at 1. Data are mean ± SD analyzed by Mann-Whitney test; *, $p < 0.05$. C) Morphology of transgenic *sobir1-12* BIR1 (L6 and L8) after a 12 day-treatment with 30 µM DEX. Note that plants exhibited WT morphology, albeit reduced rosette size due to DEX effects on plant growth. BIR1 transcripts were significantly abundant in DEX-treated *sobir1-12* BIR1 (L6 and L8). D) Rosette size (diameter) in BIR1 overexpressing ETI/PTI mutants after 12 days of DEX treatment relative to the non-treated controls. Box and whisker plots showing 5-95 percentile were analyzed by Mann-Whitney test; ****, $p < 0.0001$. Note that rosette size is largely influenced by the effect of DEX on plant development as shown for WT Col-0 plant in this study (Figure S2).